OXFORD

SOT | Society of Toxicology
www.toxsci.oxfordjournals.org

TOXICOLOGICAL SCIENCES, 157(1), 2017, 112–128

doi: 10.1093/toxsci/kfx025
Advance Access Publication Date: January 25, 2017
Research article

The Minipig is a Suitable Non-Rodent Model in the Safety Assessment of Single Stranded Oligonucleotides

Annamaria Braendli-Baiocco,*[,1,2] Matthias Festag,*[,1] Kamille Dumong Erichsen,† Robert Persson,† Michael J. Mihatsch,‡ Niels Fisker,† Juergen Funk,* Susanne Mohr,* Rainer Constien,§ Corinne Ploix,* Kevin Brady,* Marco Berrera,* Bernd Altmann,* Barbara Lenz,* Mudher Albassam,¶ Georg Schmitt,* Thomas Weiser,* Franz Schuler,* Thomas Singer,* and Yann Tessier†

*Roche Pharmaceutical Research and Early Development, Pharmaceutical Sciences, Roche Innovation Center Basel, F. Hoffmann-La Roche Ltd, 4070 Basel, Switzerland; †Roche Pharmaceutical Research and Early Development, Pharmaceutical Sciences, Roche Innovation Center Copenhagen, Hørsholm 2970, Denmark; ‡University Hospital Basel, Institute for Pathology, Basel 4031, Switzerland; §Roche Pharmaceutical Research and Early Development, Bioanalytical Research and Development, Roche Innovation Center Munich, Roche Diagnostics GmbH, Penzberg 82377, Germany; and ¶Roche Pharmaceutical Research and Early Development, Pharmaceutical Sciences, Roche Innovation Center New York, F. Hoffmann-La Roche Ltd, New York, New York 10016, USA

[1]These authors contributed equally to this study.

[2]To whom correspondence should be addressed at Roche Pharmaceutical Research and Early Development, Pharmaceutical Sciences, Roche Innovation Center Basel, F. Hoffmann-La Roche Ltd, Grenzacherstrasse, 4070 Basel, Switzerland. Fax: +41 61-68-81-01. E-mail: annamaria.braendli-baiocco@roche.com.

ABSTRACT

Non-human primates (NHPs) are currently considered to be the non-rodent species of choice for the preclinical safety assessment of single-stranded oligonucleotide (SSO) drugs. We evaluated minipigs as a potential alternative to NHPs to test the safety of this class of compounds. Four different phosphorothioated locked nucleic acid-based SSOs (3 antisense and 1 anti-miR), all with known safety profiles, were administered to minipigs using similar study designs and read-outs as in earlier NHP studies with the same compounds. The studies included toxicokinetic investigations, in-life monitoring, clinical and anatomic pathology. In the minipig, we demonstrated target engagement by the SSOs where relevant, and a similar toxicokinetic behavior in plasma, kidney, and liver when compared with NHPs. Clinical tolerability was similar between minipig and NHPs. For the first time, we showed similar and dose-dependent effects on the coagulation and complement cascade after intravenous dosing similar to those observed in NHPs. Similar to NHPs, morphological changes were seen in proximal tubular epithelial cells of the kidney, Kupffer cells, hepatocytes, and lymph nodes. Minipigs appeared more sensitive to the high-dose kidney toxicity of most of the selected SSOs than NHPs. No new target organ or off-target toxicities were identified in the minipig. The minipig did not predict the clinical features of human injection site reactions better than the NHPs, but histopathological similarities were observed between minipigs and NHPs. We conclude that there is no impediment, as default, to the use of minipigs as the non-rodent species in SSO candidate non-clinical safety packages.

Key words: locked nucleic acid; minipig; non-human primate; single-stranded oligonucleotide; safety assessment.

© The Author 2017. Published by Oxford University Press on behalf of the Society of Toxicology.
This is an Open Access article distributed under the terms of the Creative Commons Attribution-NonCommercial-NoDerivs licence (http://creativecommons.org/licenses/by-nc-nd/4.0/), which permits non-commercial reproduction and distribution of the work, in any medium, provided the original work is not altered or transformed in any way, and that the work properly cited. For commercial re-use, please contact journals.permissions@oup.com

Single-stranded oligonucleotides (SSO) are oligomers of synthetic nucleotides, typically 12–20 bases in length and designed to hybridize to complementary RNA. Historically, the first key modification of therapeutic SSOs was the introduction of a phosphorothioated backbone, and more recent developments included modifications of the sugar moieties, eg, locked nucleic acids (LNAs). These modifications were shown to improve stability, target affinity and potency, and to reduce non-specific toxicities (Veedu *et al.*, 2010; Vester and Wengel, 2004). Although numerous SSOs are currently being evaluated in clinical trials for various therapeutic indications, up to now only 2 SSO drugs have been approved (FDA Briefing Document, 2012; Perry and Balfour, 1999).

Upon parenteral administration, SSOs distribute broadly and are rapidly cleared from the circulation. After repeated dosing, they tend to accumulate in tissues, with the highest levels found in the kidney and liver, followed by lymphoid and other tissues, a characteristic observed across different mammalian species (Geary *et al.*, 2015). SSO-mediated toxicities are categorized into Watson/Crick hybridization-dependent effects, caused by on-target effect (exaggerated pharmacology) or off-target (secondary) pharmacology, and potential non-hybridization related toxicities (Frazier, 2015). SSO accumulation-related effects, pro-inflammatory effects or protein binding of the SSO may be examples of those hybridization-independent toxicities. In plasma, they may manifest as an acute and transient prolongation of coagulation and/or activation of the alternative complement system, particularly following intravenous administration in the non-human primate (NHP), upon reaching high plasma exposures (Crooke *et al.*, 2016). In addition, renal tubular cell degeneration, glomerulonephritis, hepatic toxicity with increased serum aminotransferase activities, single cell necrosis of hepatocytes, as well as thrombocytopenia and injection site reactions (ISRs) after subcutaneous administration may be identified during preclinical and/or clinical investigations (Burdick *et al.*, 2014; Engelhardt *et al.*, 2015; Frazier, 2015; Henry *et al.*, 1997; van Meer *et al.*, 2016). These toxic effects may be hybridization-dependent or -independent and are generally sequence-specific and related to tissue exposures.

Currently, there are no specific guidelines regulating the approval process of SSO drug candidates. As they are chemically synthesized, international guidelines for small molecules are followed that require repeat-dose toxicity studies to be conducted in both a rodent and non-rodent species (ICH M3[R2]) for advancing SSOs into the clinics. The selection of an appropriate animal species is essential in safety studies (Morton, 1998). Due to high genomic homology and pharmacokinetic similarities with humans, the cynomolgus monkey has been the non-rodent species of choice for the preclinical assessment of SSO safety and is considered predictive for identifying potential toxicities in humans.

Recent investigations have confirmed the minipig as a suitable alternative non-rodent model in safety studies, and there is evidence supporting the predictive validity of minipigs in the preclinical development of pharmaceuticals (Bode *et al.*, 2010; Ganderup *et al.*, 2012). The minipig shows many similarities to human anatomy, physiology, and biochemistry (Forster *et al.*, 2010). It is already widely used in the safety assessment of pharmaceuticals for topical dermal delivery as its skin resembles the human skin like no other non-rodent species does (Mahl *et al.*, 2006). Given the high incidence of ISRs in humans receiving subcutaneous administrations of SSOs (van Meer *et al.*, 2016), and the limited predictivity of rats and NHPs for these local effects identified clinically, we set out to investigate if the minipig could be a more predictive model for ISRs. To date only a scarce dataset on the use of the minipig in SSO safety assessment is publicly available. In single studies, SSOs were administered either intradermally (Cai *et al.*, 2012), intravitreally (Danis *et al.*, 2003), subcutaneously (Iyer *et al.*, 2002), or topically (Mehta *et al.*, 2000). With the recent sequencing of its genome (Heckel *et al.*, 2015; Vamathevan *et al.*, 2013), the minipig may now enable the design of cross-species reactive SSOs and the assessment of pharmacology-related adverse effects.

Here, we aimed to characterize the minipig in comparison to NHPs through short-term safety studies using parenteral routes, and including pharmacokinetic and pharmacodynamic profiling. These studies were conducted on four LNA-based SSOs (3 with mRNA targets and 1 targeting a microRNA) that had been tested in rodents, NHPs, and humans. Applying the principles of 3Rs (Russell *et al.*, 1959), only female minipigs were used as there were no gender differences in drug response reported neither in NHPs nor in humans.

We thus have, for the first time, investigated the toxicity profile of these molecules in minipigs following systemic administration.

MATERIALS AND METHODS

LNA SSO Selection and Study Design

We selected three different antisense LNA SSOs with a phosphorothioate backbone, previously characterized in NHPs and humans (Durig *et al.*, 2011; Frieden and Orum, 2008; Lee *et al.*, 2013; Lindholm *et al.*, 2012; Straarup *et al.*, 2010; van Poelgeest *et al.*, 2013) and a LNA-based microRNA antagonist, with a phosphorothioate backbone (Gebert *et al.*, 2014; Hildebrandt-Eriksen *et al.*, 2012).

The SSOs were administered to female minipigs applying a study design similar to the reference NHP studies, including toxicokinetic investigations, in-life monitoring, clinical, and anatomic pathology. In addition, immunohistochemistry, *in situ* hybridization, and transmission electron microscopy (TEM) were performed in minipig samples to localize the SSOs in target organs, to confirm target engagement and evaluate changes ultrastructurally.

Oligonucleotides Design and Synthesis

The four selected molecules are phosphorothioated LNA-based SSOs with the following characteristics:

RTR5001—Targets the proprotein convertase subtilisin/kexin type 9 (PCSK9) mRNA (NCBI reference sequence: NM_174936.3) with the sequence 5′-TGCtacaaaacCCA-3′ (uppercase LNA, lowercase DNA). It matches the sequence of humans and cynomolgus monkeys and has a single, end-standing mismatch to the minipig sequence.

RTR4955—Antagonist of the Apolipoprotein B-100 (APOB) mRNA (NCBI reference sequence: NM_000384.2) with the sequence 5′-GTtgacactgTC-3′. It matches the sequence of humans and cynomolgus monkeys and has a single, mid-standing mismatch to the minipig sequence.

RTR3649—A mixed LNA/DNA phosphorothioated microRNA 122 biogenesis modulator, with the sequence 5′-CcAttGTcaCaCtCC-3′. It has a full match to the human, cynomolgus monkey, and minipig sequences.

RTR2996—Binds and inactivates the B-cell-lymphoma 2 (BCL-2) oncoprotein mRNA (NCBI reference sequence NM_000633.2 and NM_000657.2) with the sequence 5′-CTcccaacgtgcgCCa-3′ (Stein *et al.*, 2010) and has a single, mid-

standing mismatch to the human, cynomolgus monkey and minipig sequences.

All four LNA SSOs were synthesized according to standard protocols as previously described (Lindholm *et al.*, 2012; Straarup *et al.*, 2010), were characterized, and ultimately diluted with 0.9% NaCl to the required concentrations. LNA SSO formulations contained ≤7% impurities, and the presence of endotoxins was excluded.

Animals

Purpose-bred female Göttingen minipigs were supplied by Ellegaard (Dalmose, Denmark). The minipigs were aged between 4 and 6 months at study start and were pair-housed in pens approximately 9 m^2 in size. Animals were offered environmental enrichment and were kept at 20 ± 2 °C at a relative humidity of 40–80% with a 12-h light/dark cycle in a facility accredited by the Association for Assessment and Accreditation of Laboratory Animal Care International (AAALAC). Animals were allocated to groups, avoiding sister–sister relationships. Animals were regularly monitored, offered a standard minipig diet, and tap water *ad libitum*. Only female minipigs were used as no gender differences in drug response had been reported in NHPs or humans. All procedures were in accordance with the respective Swiss regulations and approved by the Cantonal Ethical Committee for Animal Research.

Clinical observations, body weight development, and food consumption were closely monitored throughout the study.

Experimental Groups

RTR5001 and RTR4955—Three animals per group and dose level received a subcutaneous dose (inguinal region, left and right alternated) of 6 or 20 mg/kg RTR5001 or 8 or 24 mg/kg RTR4955, respectively, on days 1, 6, 11, and 16 at a dose volume of 0.25 mL/kg. Two females per compound received phosphate-buffered saline (PBS) and were used as concurrent controls.

RTR3649—A subcutaneous dose (caudal to the pinna, left and right alternated) was administered to three females per group at 3, 12, and 48 mg/kg twice per week (a total of 9 doses over 4 weeks) at a dose volume of 0.32 mL/kg. Three female minipigs received sterile physiological saline and were used as concurrent controls. Reversibility of findings was assessed after a 4-week dosing-free period in two additional control and two high-dose minipigs.

RTR2996—Three minipigs were dosed intravenously at 5, 15, and 45 mg/kg RTR2996 for 5 min at 2 mL/kg every other day for 15 days. Three control females were given sterile physiological saline. A 14-day dosing-free period was planned in 2 additional control and 2 high-dose minipigs. The RT2996 dose levels for the minipig were reduced by 1/3 compared to NHP, aiming for comparable liver exposures, based on a preliminary single-dose pharmacokinetic study. Drug or saline were administered intravenously via a vascular access port (VAP) that was implanted approximately 4 weeks prior to the start of the study. The VAP was implanted in the external jugular vein, with the catheter tip being positioned in the *vena cava cranialis*. The catheter was tunneled subcutaneously and connected to the port chamber located caudal to the pinna. Following the procedure, animals were closely monitored and received post-operative care.

Exposure Assessment

For RTR5001 and RTR4955, blood was collected for plasma exposure assessment at several time points after dosing on day 1 and throughout the study. For RTR3649, blood was collected up until 72 h and for RTR2966 up until 48 h after the first and last doses. In addition, liver and kidney cortex tissue samples were collected during necropsy. Samples were analyzed with dedicated, qualified hybridization enzyme-linked immunosorbent assays (hELISAs) (Hildebrandt-Eriksen *et al.*, 2012; Straarup *et al.*, 2010). Plasma exposure data were subjected to non-compartmental pharmacokinetic evaluation and mean C_{max} and area under the curve (AUC) values were determined.

Clinical Pathology

Blood was sampled on different occasions for assessment of a full set of hematology, coagulation, and clinical chemistry parameters as well as cytokines and complement. Cytokines (IFN-α, IFN-γ, IL-1b, IL-2, IL-4, IL-6, IL-8, IL-10, and TNF-α) were assessed prior to dosing and at 2 and 7–8 h after dosing). For RTR2996, total complement activity (CH50) was assessed on day 15 before dosing and at 0.25 h and 24 h after dosing. Additionally, urine was collected in a metabolic cage for 16 h (RTR5001 and RTR4955) or for 24 h (RTR3649 and RTR2996), before first dosing and towards the end of the dosing period. Hematology parameters were determined using a Sysmex® XT instrument (Sysmex, Japan), coagulation parameters with ACL TOP500 (Instrumentation Laboratory, USA), and clinical chemistry parameters with an Advia 180 (Siemens) automated system. Urinary chemistry parameters were measured with an Aution Max™ AX-4280 instrument (Arkray Clinical Diagnostics, USA) and an Advia 1800 (Siemens) automated system. Cytokines were determined by ELISA using the Porcine Cytokine Chemiluminescent 9-plex Array Kit on an AS0034 Imager with the SignaturePLUS™ imaging system and the PROarray analysis software (all Aushon SearchLight, USA) according to provider's instructions. In the results significantly altered parameters when compared with control and/or pretest values are presented.

Necropsy and Anatomic Pathology

All animals were sacrificed 24 h after the last dose. A complete post-mortem examination was performed and an extensive list of tissues and organs (limited list for RTR3649) were fixed by immersion in 10% buffered formalin, embedded in paraffin, and blocked. The tissue blocks were sectioned at 5 μm, stained with hematoxylin and eosin (H&E). The kidney histologic sections were additionally stained with Periodic acid–Schiff (PAS). Slides were microscopically evaluated and representative slides or scans from slides from NHP studies were reviewed by the same toxicologic pathologist.

Immunohistochemistry, *in-Situ* Hybridization and Transmission Electron Microscopy

Immunohistochemistry—Immunohistochemistry to localize SSOs was performed using a Ventana Discovery XT® immunostainer (Ventana Medical Systems, Tucson, AZ). Formalin-fixed and paraffin-embedded tissue sections of kidney, liver, and lymph nodes (3–4 μm thick) of selected animals were de-paraffinized and an anti-SSO pAb2 rabbit polyclonal antibody (synthesized *ad hoc* by Creative Biolabs) diluted 1:100 was used as a primary antibody in a standard protocol using the Ventana Red MAP® kit (Ventana, 760-123). A Biotin-SP-conjugated AffiniPure donkey anti-rabbit IgG antibody diluted 1:200 (Jackson ImmunoResearch, 711-065-152) was used as secondary antibody. Sections were stained with Fast Red and counterstained

with hematoxylin. Rabbit serum (Dako, X0902) was used as a negative control. In addition, lysosome-associated membrane glycoprotein-2 (LAMP-2) immunohistochemistry was performed on selected kidney histological sections using a polyclonal rabbit anti-LAMP-2 antibody (Thermo Scientific, 51-2200) diluted 1:50 in a standard protocol using the Ventana DAB MAP® kit (Ventana, 760-124). A Biotin-SP-conjugated AffiniPure donkey anti-rabbit IgG (Jackson Immuno Research, 711-065-152) diluted 1:100 was used as secondary antibody. Sections were stained with 3,3′-diaminobenzidine (DAB) and counterstained with hematoxylin.

In-situ hybridization—*In-situ* hybridization was used to detect and localize RTR5001 in kidney, liver, and lymph node tissue samples of individual animals. Formalin-fixed and paraffin-embedded tissue sections (3–4 μm thick) were de-paraffinized and pre-treated with protease. A digoxigenin-labelled complementary LNA probe to RTR5001 was designed and provided by Exiqon. Following hybridization, sections were stained with DAB and counterstained with hematoxylin. All steps of this procedure were carried out using a Ventana Discovery Ultra® immunostainer. An unlabeled LNA probe against proprotein convertase subtilisin/kexin type 9 (PCSK9) and LNA digoxigenin-labeled U6 (provided by Exiqon) were used as negative and positive controls, respectively, for each case. Specific staining signals were identified as brown, punctate dots or diffuse staining present in the cytoplasm. In addition, mRNA *in-situ* hybridization was applied to investigate the downregulation of PCSK9 and APOB mRNA in liver tissue samples after dosing with RTR5001 and RTR4955, respectively. PCSK9 and APOB mRNA were visualized in formalin-fixed and paraffin-embedded liver samples (Wang *et al.*, 2012) using RNAscopeVS® (Advanced Cell Diagnostics). Liver tissue sections (3–4 μm thick) were de-paraffinized and treated with protease. PCSK9- or APOB-specific mRNA target probe sets ($N = 20$) for *Sus scrofa* were provided by Exiqon (gene ID 100620501, targeted bps 2 through 1464 of the PCSK9 cDNA sequence; Gene ID 100523371, targeted bps 3564 through 4553 of the APOB cDNA sequence). Following signal amplification, sections were stained with Fast Red and counterstained with hematoxylin as previously described (Atzpodien et al., 2016). All steps of this procedure were carried out using a Ventana Discovery Ultra® immunostainer. Probes to the bacterial gene dapB and the endogenous UBC mRNA were used as negative and positive controls, respectively. Specific staining signals were identified by light microscopy as red, punctate dots in the cytoplasm.

Transmission electron microscopy—For TEM, kidney samples from controls and RTR4955-treated minipigs were fixed in 3.5% glutaraldehyde at room temperature, osmicated, and embedded in epoxy resin. Ultra-thin sections were cut, collected on grids, counterstained with uranyl acetate and lead citrate and examined using a transmission electron microscope.

Tissue Quantitative PCR Analysis

Total RNA was extracted from flash-frozen liver samples using the RNeasy mini kit (Qiagen). RNA integrity number (RIN) was checked with the Agilent 2100 Bioanalyzer System and RNA was subsequently transcribed into cDNA. Expression levels of APOB and PCSK9 were determined by quantitative PCR using commercially available reagent and TaqMan assays (ThermoFisher). Gene expression levels were normalized against the housekeeping gene beta glucuronidase (GUSB).

Statistical Analyses

Group means and standard deviations (SD) were calculated for $N \geq 3$ minipigs per group using Provantis software (Instem Life Sciences, Stone, UK). Differences between the control group and treated groups were determined using an ANOVA with Dunnett's multiple comparison test. Values of $P < .05$ were considered statistically significant.

RESULTS

Exposure Assessment and Tissue Biodistribution

After RTR5001, RTR4955, and RTR3649 administration, the plasma exposure, AUC and C_{max} values increased roughly or slightly more than dose-proportionally. For RTR2996, $AUC_{0\text{-}24h}$ and C_{max} values increased less than dose-proportionally between 15 and 45 mg/kg. Plasma exposure over repeated administrations at the high dose increased for RTR4955 and RTR2996 but remained unchanged for RTR5001 and RTR3649. All tested SSOs were rapidly cleared from the blood circulation, resulting in a concentration 2–3 orders of magnitude lower than the C_{max} after 24 h. RTR4955 kidney exposure was similar at 8 and 24 mg/kg. RTR2996 tissue levels increased with dose from 5 to 15 mg/kg and showed a trend for saturation at 45 mg/kg. An exposure saturation in kidney and liver tissue was also identified at 48 mg/kg for RTR3649. Liver tissue levels increased dose-dependently after RTR5001 and RTR4955 administration, as did kidney levels with RTR5001. Generally, the four investigated SSOs partitioned to a markedly higher concentration in the kidney cortex than in the liver (Supplementary Table 1 and Figs 1–3).

In-Life Observations and Clinical Pathology

RTR5001—All animals survived up to the scheduled sacrifice. There were no RTR5001-related clinical signs or ISRs and no change in hematology, coagulation parameters and cytokines was observed. On day 17 at 20 mg/kg, one minipig had a concomitant increase in serum creatinine (1.6-fold) and blood urea nitrogen (BUN; (1.8-fold); another minipig showed an increase in BUN only (1.2-fold).

Urinary changes at 20 mg/kg consisted of an increase in urinary volume with concomitant increase of N-acetyl-beta-D-glucosaminidase (NAG) and calcium (Ca) normalized to creatinine. There were no changes in urinary protein levels.

A statistically significant ($P < .05$) decrease (up to −53%) in mean serum low-density lipoprotein (LDL), accompanied by a decrease of mean total cholesterol serum (−20 to 30%), was observed on days 12 and 17 and decreased triglyceride levels on day 17 in the 20 mg/kg group, which are expected pharmacologic effects.

RTR4955—One minipig at 24 mg/kg was sacrificed for humane reasons on day 15 approximately 96 h after the third dose and 2 days prior to its scheduled sacrificing. It presented with a markedly decreased food consumption, an acute loss in body weight (7% decrease vs the highest previously recorded value) and clinical signs (hypoactivity and tremors). All other animals showed a marginal reduction of body weight gain without concomitant changes in food consumption. Neither ISRs nor changes in cytokine values were seen in any animal.

Neutrophil (2-fold) and monocyte (2.7-fold) counts as well as fibrinogen (2.2-fold) levels were significantly ($P < .001$) increased in minipigs at 24 mg/kg on day 17. Serum aspartate aminotransferase (AST) and glutamate dehydrogenase (GDH) activities were significantly ($P < .05$) increased by up to 2-fold

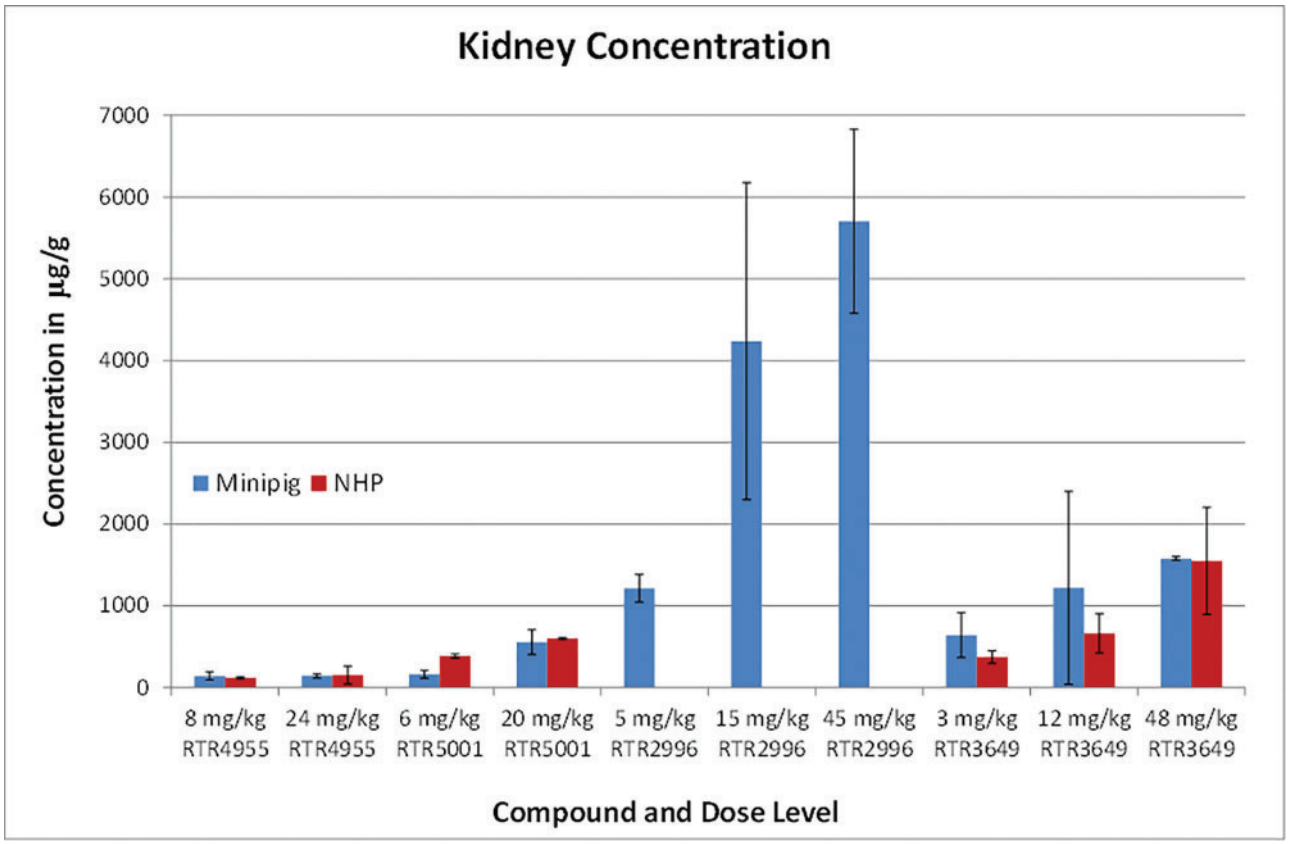

FIG. 1. Mean exposure levels in the kidney cortex after repeated subcutaneous (RTR5001, RTR4955, or RTR3649) or intravenous (RTR2996) administration to minipigs or NHPs ($N = 3$ or $N = 5$ with ±SD) at different dose levels. NHPs were dosed intravenously with RTR3649; no kidney samples were collected from NHPs after RTR2996 administration. Similar dose:exposure relationships were observed in the kidney cortex with all four tested LNA SSOs.

on day 17 at 24 mg/kg. Creatinine and BUN concentrations were increased in all RTR4955-dosed minipigs by up to 48% and 2-fold, respectively on day 17, starting earlier in animals at 24 mg/kg.

Urinary changes included increases in urinary volume, protein as well as NAG, sodium (Na), Ca and chloride (Cl) concentrations normalized to creatinine, in animals dosed at 24 mg/kg. Urinary protein was also increased in one animal dosed at 6 mg/kg. Parameters that would indicate a pharmacodynamic effect, eg, total cholesterol, LDL or high-density lipoprotein (HDL) concentrations, were not altered.

RTR3649—All animals survived to the scheduled sacrificing. There were no RTR3649-related clinical signs, ISRs, or changes in hematology and urinary parameters. Marginally increased prothrombin time (PT; 10–26%) and activated partial thromboplastin time (APTT; up to 18%) values in minipigs at 12 and 48 mg/kg were observed after repeated administration on days 16, 25, and 30.

On day 16, the total cholesterol level was decreased by 16% in minipigs dosed at 48 mg/kg; a decrease was also observed in an individual animal on day 30. This was accompanied by a minimal decrease in HDL cholesterol at days 16 and 30 (reductions of 19% and 26% at 12 mg/kg, and 33% and 31% at 48 mg/kg, respectively). In addition, serum triglyceride levels were statistically significantly decreased at days 16 and 30 (decreases of 50% and 58% at 12 mg/kg, and 62% and 64% at 48 mg/kg, respectively) when compared with control and/or pretest values. After the dosing-free period, serum cholesterol concentration was low in 1 of the 2 animals previously dosed at 48 mg/kg; HDL and triglyceride levels were low in both minipigs. Decreases in cholesterol, HDL and triglyceride levels were expected pharmacodynamic effects of RTR3649. There were no relevant changes in cytokine levels.

RTR2996—One of the five minipigs at 45 mg/kg, which was originally assigned for evaluation during recovery, was sacrificed for humane reasons three days after the last dose. It presented a marked acute body weight loss that corresponded with reduced food consumption and hypoactivity. The overall condition of this minipig was likely due to kidney changes, which were more severe than in the other animals of this group. In addition, a discoloration (flushing) of limbs, ears and snout was observed shortly after the last dosing which was attributed to complement activation. After repeated dosing, the majority of minipigs dosed at 45 mg/kg presented with a transient flushing of limbs, ears and nose immediately after dosing. A prolonged bleeding time after blood collection was also noted. Accordingly, transient and statistically significant increases in PT and APTT were observed at 45 mg/kg after the first dose, and this became more pronounced after the last dose (mean values were about 3.5 fold higher than baseline). By 24 h after dosing, effects on coagulation parameters had partially or totally resolved (Figure 4A). Hematology changes observed at 45 mg/kg at day 16 were statistically significant (at least $P < .05$). A reduction in red blood cell (RBC; 11%) and lymphocyte counts (35%) and an increase in reticulocyte count (2.2-fold) were also observed.

At day 16, animals dosed with 45 mg/kg had slight but statistically significant ($P < .05$) increases in cholesterol (36%),

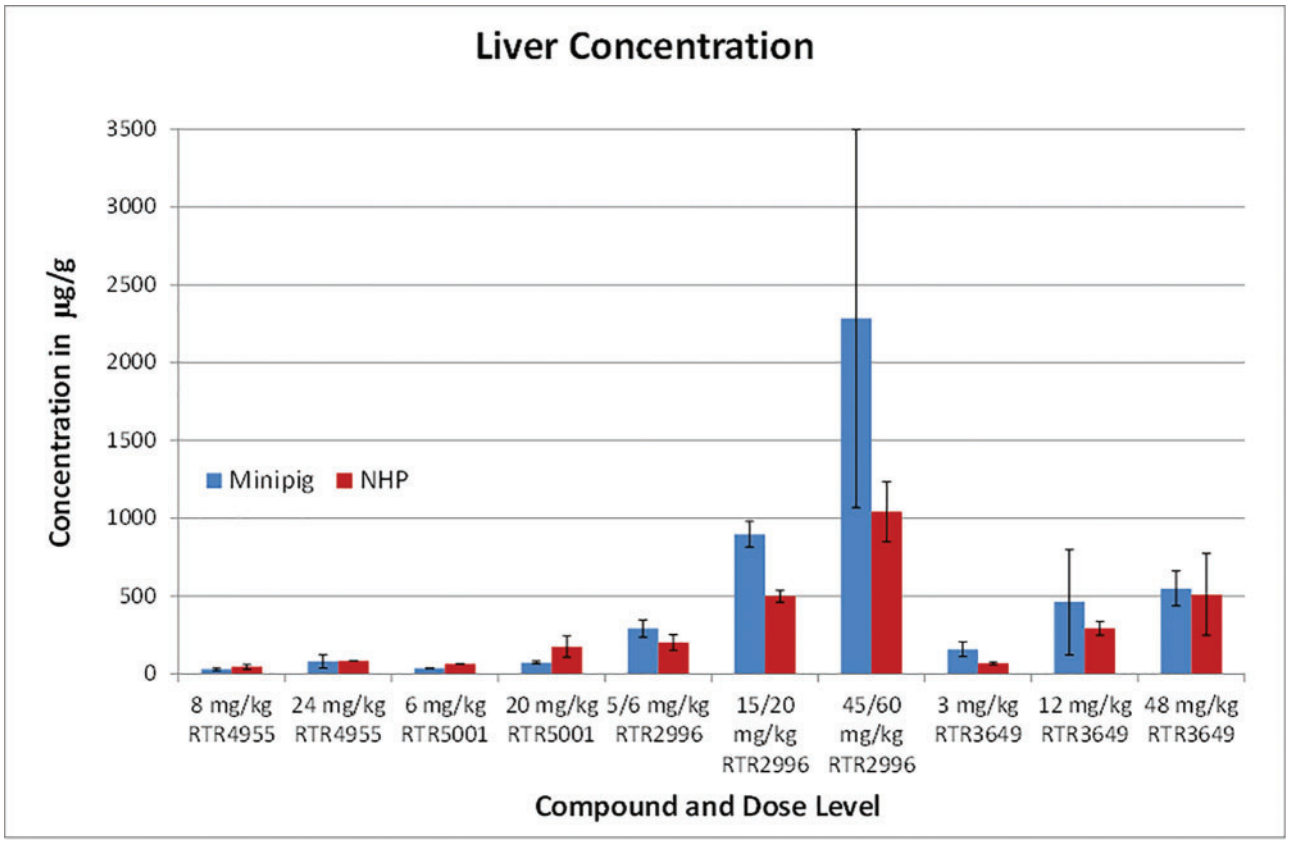

FIG. 2. Mean exposure levels in the liver after repeated subcutaneous (RTR5001, RTR4955 or RTR3649) or intravenous (RTR2996) administration to minipigs or NHPs ($N = 3$ or $N = 5$ with ±SD) at different dose levels (NHPs were dosed intravenously for RTR3649). Similar dose:exposure relationships were observed in the liver cortex with all four tested LNA SSOs.

creatinine (59%), BUN (88%), total proteins (17%), albumin (13%), globulin (28%), alanine aminotransferase (ALT; 34%), gamma glutamyltranspeptidase (GGTP; 31%) and HDL (45%) levels as well as markedly increased aspartate aminotransferase (AST; 2.8-fold) and sorbitol dehydrogenase (SDH; 9.1-fold) values. There were no changes in cytokine values. The total complement activity (CH50), as measured on day 15, was statistically significantly ($P < .05$) activated 15 minutes post-infusion in the 45 mg/kg group. CH50 levels returned nearly to baseline at 24 hours post-infusion (Figure 4B).

Urinary changes consisted of slightly increased urinary proteins in minipigs dosed at 45 mg/kg while the urinary volume was increased in one animal at 15 and 45 mg/kg each. Due to a kinked catheter, one minipig dosed at 45 mg/kg was only partially dosed, but presented similar findings as the other animals in this dose group. It was the only animal that underwent a full 14-day dosing-free period and therefore, an assessment of potential recovery of effects was not feasible.

Gross and Anatomic Pathology

At necropsy, increased kidney weights were recorded with increasing dose levels in animals that were administered the different SSOs. A pale discoloration of the kidney was observed in animals dosed with RTR5001, RTR4955 and RTR2996. A dose-dependent increase in liver weights was seen in minipigs dosed with RTR3649 and RTR2996; this was still present after the end of the treatment-free period for RTR3649. In addition, a red discoloration of the injection site was observed in several minipigs dosed with RTR5001, RTR4955, RTR3649, and controls. This discoloration generally corresponded to histopathologic findings of inflammation and acute hemorrhage.

RTR5001—Histopathological findings were identified in the kidney, liver, lymph nodes, and at the injection sites. In the kidney, mild to moderate dilatation of the proximal renal tubules accompanied by mild to moderate tubular degeneration/regeneration was seen in 2 of 3 minipigs at 20 mg/kg; this corresponded to increased kidney weights and pale discoloration at necropsy. Tubular degeneration consisted of proximal tubular cell vacuolation, necrosis of tubular cells and occasional apoptotic/necrotic cells in the lumen. The lesions involved the proximal tubules and started at the urinary pole of the glomerulus. Sometimes, the parietal epithelial cells around the urinary pole also showed vacuoles. Not all nephrons were affected to the same extent. In one of the affected minipigs, dosed at 20 mg/kg, presence of necrotic cells in the lumen was more abundant and, in some tubules, denudation of the basement membrane was observed (Figure 5A). Tubular regeneration was characterized by basophilic hypertrophied tubular cells with prominent enlarged nuclei and nucleoli and rare mitoses (as seen for RTR2996, Figure 5B). The subcapsular region of the cortex was more severely affected by the described lesions. The medulla was always unchanged. Cytoplasmic PAS negative granules were occasionally observed in the proximal tubules of minipigs dosed at 20 mg/kg.

In the liver, minimal single cell necrosis was observed in 1 of 3 minipigs dosed at 20 mg/kg (as seen for RTR2996, Figure 6A). In the mandibular, mesenteric, and inguinal (draining) lymph nodes, minimal to mild macrophage vacuolation was observed (as seen for RTR2996, Figure 6C).

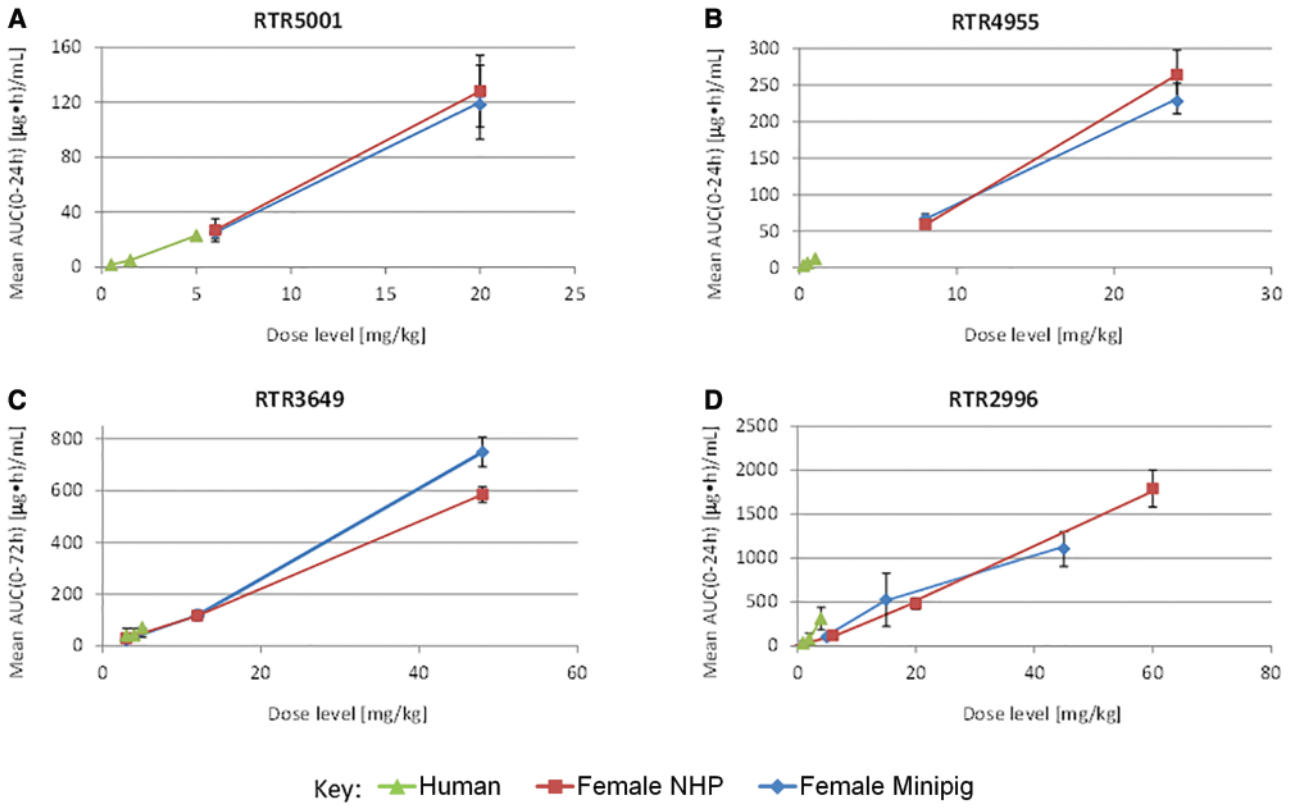

FIG. 3. Mean plasma exposure with ±SD after single administration at different dose levels. A, RTR5001, B, RTR4955, C, RTR3649, and D, RTR2996 to female minipigs (blue diamonds), female NHPs (red square) and humans (green triangle). The different species were administered subcutaneously at the indicated dose levels (except for RTR3649, where NHPs were dosed intravenously over 5 min while minipig and human subjects were dosed subcutaneously and for RTR2996 administered intravenously). The exposure was measured as AUC of plasma concentrations over a time interval of 0 to 24 h for RTR5001, RTR4955 and RTR2996 and of 0 to 72 h for RTR3649 (except for RTR3649 and RTR2996 in humans, where the time intervals were 0–96 h and 0–48 h, respectively). For the minipig, NHP and human AUC values increased roughly or slightly more than dose-proportionally for RTR5001, RTR4955, RTR3649, and RTR2996 (NHP and human only). In the minipig $AUC_{0\text{-}24h}$ values increased less than dose-proportionally for RTR2996.

At the injection site, increased subcutaneous inflammation characterized by presence of macrophages, lymphocytes and granulocytes was observed in animals dosed at 6 and 20 mg/kg when compared with controls. This inflammation was accompanied by mild subcutaneous edema, fibrin exudation and necrosis at the left injection site (injected on days 6 and 16) and was less severe and not accompanied by edema and necrosis at the right injection site (injected on days 1 and 11), demonstrating a tendency to reversibility of these lesions. In addition, minimal to moderate acute hemorrhages were observed at the injection sites of RTR5001-dosed animals.

RTR4955—In the animal prematurely sacrificed on day 15, abundant ascites, marked perirenal edema accompanied by edema of the mesentery, and hemorrhage in the kidney capsule were recorded.

Histopathologically, in the kidney, a dose-dependent tubular dilatation, degeneration and regeneration, similar to that with RTR5001 and corresponding with increased kidney weights and pale discoloration at necropsy, was identified. At 24 mg/kg, in addition to the severe tubular degeneration and regeneration, there were inflammatory cell infiltrates in the interstitial space and some hyaline casts in the tubular lumen. The animal that was sacrificed for humane reasons on day 15 also presented with abundant granulocytes in the tubules (possibly as a consequence of fibrin exudation in the glomeruli) and a mesangioproliferative glomerulonephritis with glomerular loop necrosis with fibrin exudation in the Bowman's space (Figure 5C). In addition, hepatocellular vacuolation and minimal single cell necrosis in the liver was also seen in this female.

Similarly to RTR5001, vacuolation of macrophages was observed in the mandibular, mesenteric, and inguinal (draining) lymph nodes of minipigs dosed with RTR4955.

At the injection site, hemorrhages were observed with increased severity in animals dosed with RTR4955 compared to controls. There was minimal to mild subcutaneous inflammation characterized by the presence of macrophages, lymphocytes and granulocytes in a few animals, but there was no difference in incidence between minipigs dosed with RTR4955 and controls.

RTR3649—In the kidney, cytoplasmic basophilic granules were observed in the proximal tubules of all animals dosed at 12 and 48 mg/kg. Tubular degeneration similar to those described with the other investigated LNA SSOs but of minimal to mild severity was observed in 1 of 3 minipigs at 12 mg/kg and all minipigs at 48 mg/kg. The changes were mostly localized at the or close to the urinary pole of the glomerulus, were still present after the 4-week dosing-free period and corresponded with increased kidney weights at necropsy.

In the liver, minimal or mild diffuse cytoplasmic rarefaction corresponding to an increased content of glycogen was observed in all minipigs at 12 mg/kg and in 2 of 3 minipigs at 48 mg/kg. Rarefaction of hepatocytes persisted after the 4-week treatment-free period. In addition, basophilic granules

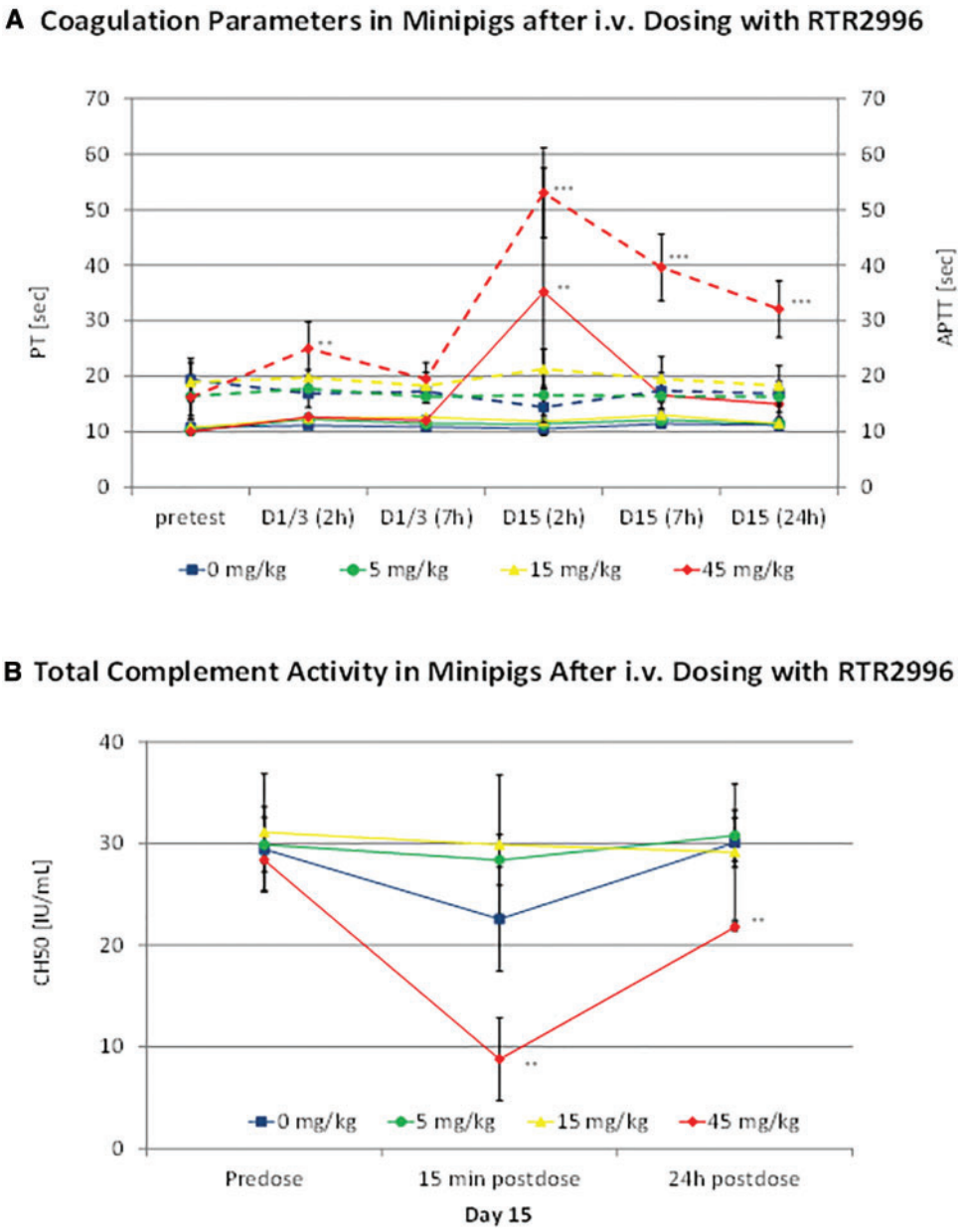

FIG. 4. Coagulation and complement activation data for minipigs ($N = 3$ or $N = 5$ with ±SD) dosed intravenously with 0, 5, 15, or 45 mg/kg RTR2996 (5 min infusion time) every other day for 15 days A, Time course of Activated Partial Thromboplastin Time (APTT; dashed lines) and Prothrombin Time (PT; solid lines) levels, on x-axis time of blood sampling for measurement of coagulation parameters, predose – baseline levels, D – days of study and in brackets hours after dosing. Transient and statistically significant increase in PT and APTT were observed at 45 mg/kg RTR2996 that were partially or totally resolved at 24 h post dose. B, Total complement (CH50) activity measured in minipig serum. Differences between the control group and groups dosed with LNA SSOs were determined using an ANOVA with Dunnett's multiple comparison tests. $^{*}P < .05$, $^{**}P < .01$ and $^{***}P < .001$ compared to control. CH50 was statistically significantly reduced 15 min post-infusion at 45 mg/kg RTR2996.

were observed in the Kupffer cells of 1 of 3 minipigs dosed at 48 mg/kg.

At the injection site, minimal to mild perivascular inflammatory cell infiltrate mainly consisting of lymphocytes with some eosinophilic granulocytes was observed in 2 of 3 minipigs dosed at 3, 12, and 48 mg/kg. In all animals at 48 mg/kg this change was accompanied by an increase of inflammatory cell infiltrate, mainly lymphocytic in the subcutis. There were mild subcutaneous fat necrosis, mild to moderate fibroplasia and increased incidence and severity of hemorrhage. In addition, macrophages with granular basophilic cytoplasm were observed in animals at 48 mg/kg. The changes at the injection site were almost completely reversible.

RTR2996—Histopathologically, in the kidney, dose-dependent tubular dilatation, degeneration, and regeneration were observed at 15 and 45 mg/kg; these effects were similar to those observed with the other investigated LNA SSOs. Hyaline casts in the tubules were identified in 2 minipigs dosed at 45 mg/kg. Basophilic fine granules in the cytoplasm of the proximal tubular epithelium (Figure 5B) were observed with a dose-dependently increased severity in animals at 15 and 45 mg/kg.

In the liver, basophilic granules in Kupffer cells (Figure 6A) and mild to moderate hepatocellular hypertrophy were observed in animals dosed at 15 and 45 mg/kg. This was accompanied by single cell necrosis/apoptosis and Kupffer cell hyperplasia in animals dosed at 45 mg/kg. In the mandibular

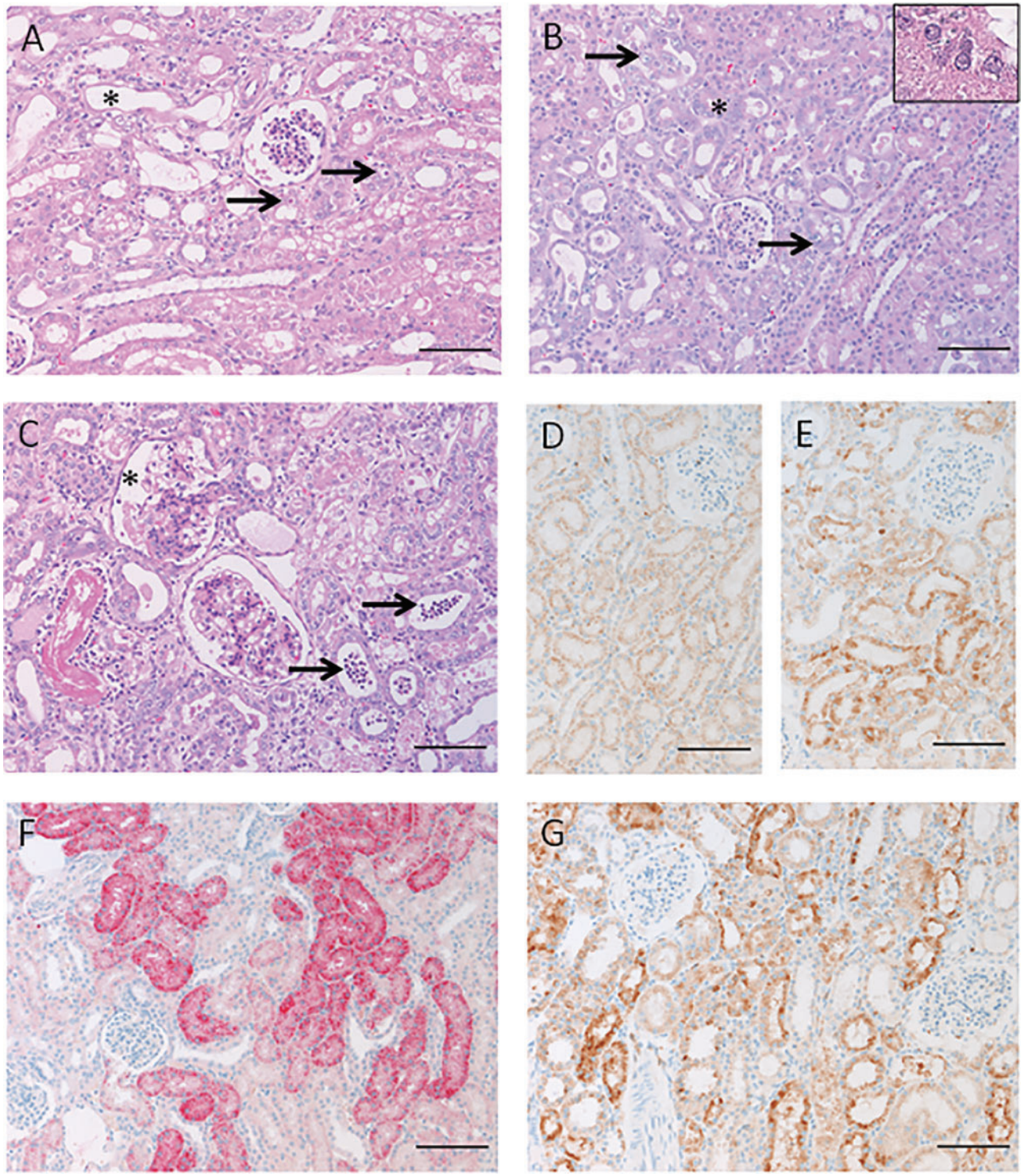

FIG. 5. Histopathologic findings in minipigs. A, Kidney, H&E. Necrosis of tubular cells (arrowheads), tubular degeneration and dilatation with denudation of basal membrane (asterisk); 20 mg/kg RTR5001. B, Kidney, H&E. Basophilic granules in proximal tubular cells (arrowheads and insert) and regeneration of proximal tubular cells (asterisk); 45 mg/kg RTR2996. C, Kidney, H&E. Mesangioproliferative glomerulonephritis and fibrin exudation into Bowman's space (asterisk); dilated tubules with many granulocytes (arrowhead); 24 mg/kg RTR4955. D, Kidney of control minipig, immunohistochemistry for LAMP-2. Presence of LAMP-2 positive structures (lysosomes) in proximal tubular cells. E, Kidney of dosed minipig, immunohistochemistry for LAMP-2. Increased number and size of positive LAMP-2 structures (lysosomes) in proximal tubular cells; 8 mg/kg RTR4955. F) Kidney, immunohistochemistry for LNA SSO. Accumulation of LNA SSO into the proximal tubular cells (red staining); 6 mg/kg RTR5001. G, Kidney, *in-situ* hybridization for RTR5001. Accumulation of LNA into the proximal tubular cells (brown staining); 6 mg/kg RTR5001 (scale bars = 100 μm, figure C scale bar = 50 μm).

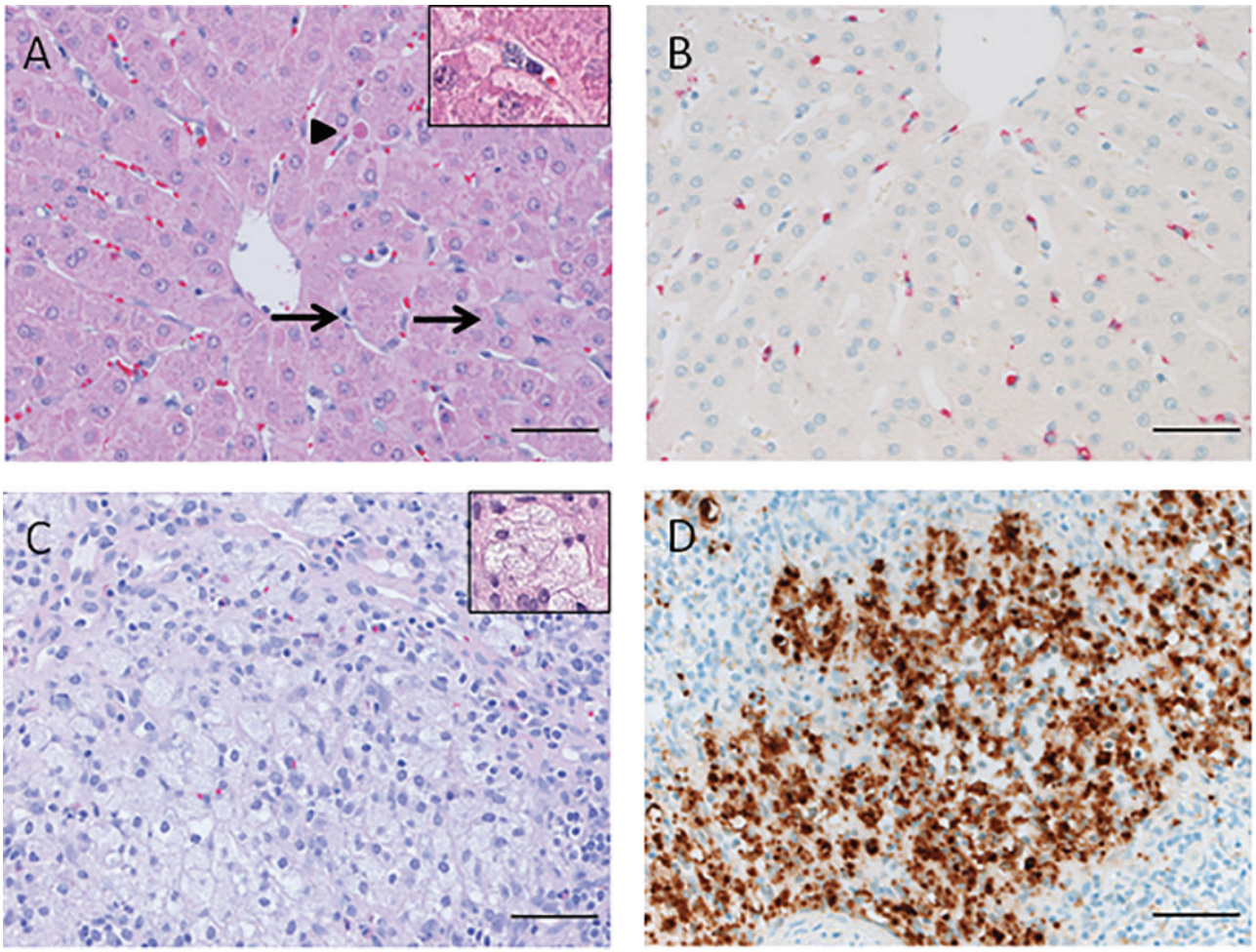

FIG. 6. Histopathologic findings in minipigs. A, Liver, H&E. Basophilic granules in Kupffer cells (long arrowheads and insert) and apoptotic hepatocytes (short arrowheads); 45 mg/kg RTR2996. B, Liver, immunohistochemistry for LNA SSO. Accumulation of LNA SSO (red staining) in Kupffer cells; 24 mg/kg RTR4955. C, Lymph node, H&E. Vacuolated macrophages (insert); 15 mg/kg RTR2996. D) Lymph node, immunohistochemistry for LNA. Accumulation of LNA SSO in the vacuolated macrophages (brown staining); 20 mg/kg RTR5001 (scale bars = 50 μm).

and mesenteric lymph nodes, vacuolated macrophages, similar to those observed with RTR5001 and RTR4955, were seen in all RTR2996-dosed groups (Figure 6C).

Immunohistochemistry, *in-Situ* Hybridization and Transmission Electron Microscopy

The presence of the different LNA SSOs was demonstrated by immunohistochemistry in the cytoplasm of tubular epithelial cells of the kidney (Figure 5F for RTR5001), in the Kupffer cells of the liver (Figure 6B for RTR4955), and in the cytoplasm of macrophages of lymph nodes (not shown). In addition, the localization of RTR5001 in the cytoplasm of tubular epithelial cells of the kidney (Figure 5G), in the Kupffer cells of the liver (not shown) and in the cytoplasm of macrophages of lymph nodes (Figure 6D) was confirmed by *in-situ* hybridization.

Immunohistochemistry revealed an increased number and size of positive LAMP-2 structures (lysosomes) in tubular epithelial cells of animals dosed with RTR4955 when compared with controls (Figure 5D and E). This confirmed the lysosomal involvement in the accumulation of the LNA SSOs.

Proximal tubular changes were similar for all four LNA SSOs at histopathologic examination and therefore tissue from one animal, dosed with RTR4955 and diagnosed with tubular lesions and mesangioproliferative glomerulonephritis, was selected for further characterization by TEM. Ultrastructurally, an increased number and size of lysosomes (Figure 7A), with storage of heterogenous osmiophilic material in the cytoplasm, was observed in the proximal tubular cells of this minipig, which was dosed with 24 mg/kg RTR4955. In addition, some tubules had variable damage from single cell necrosis to necrosis of the whole tubular cross section (Figure 7B). In the surrounding of highly affected tubules, massive edema was present in the interstitial space. Cortical collecting ducts were not affected. The glomerular structure, the basement membranes, endothelial cells or podocytes were not affected by LNA SSO dosing in the examined minipigs. One minipig, however, dosed with RTR4955 at 24 mg/kg, histopathologically presented with a mesangioproliferative glomerulonephritis. Ultrastructurally, the endothelial cells and/or mesangial cells of the glomeruli of this animal were increased or swollen and showed signs of storage of a homogenous or slightly polymorphic material, or vacuoles (Figure 7C). No electron dense deposits were observed.

Target Engagement and Pharmacodynamics

PCSK9 mRNA expression levels in minipig livers were markedly and dose-dependently reduced by up to 72% after subcutaneous

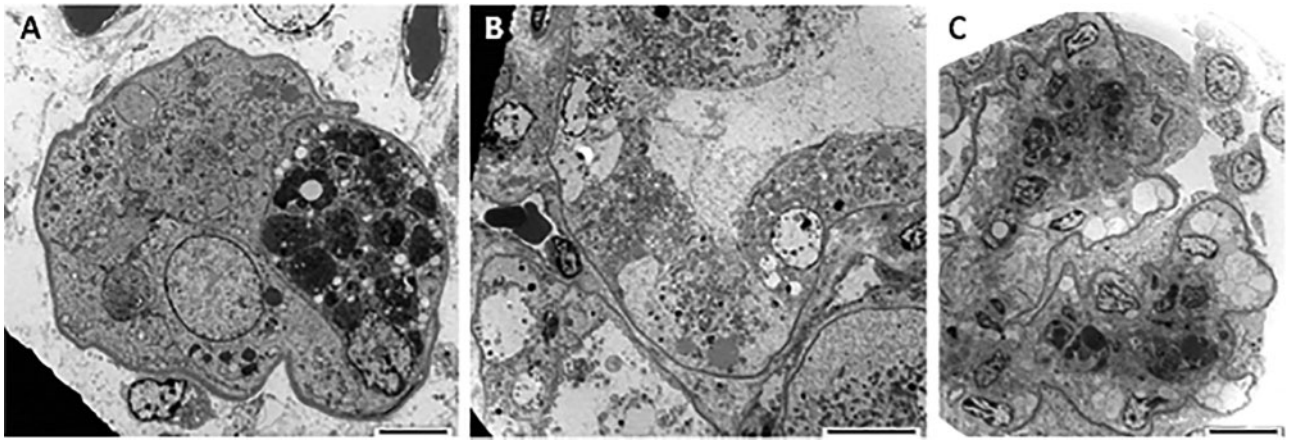

FIG. 7. Electron microscopy of kidney from a minipig dosed at 24 mg/kg RTR4955. A, Part of a tubule with massively increased number and size of lysosomes (bar = 5 μm). B, Proximal tubular degeneration and necrosis (bar = 10 μm). C, Same kidney as shown by light microscopy in Figure 5C. Mesangioproliferative glomerulonephritis with prominent mesangial hypercellularity and lysosomal inclusion in mesangial cells. Note: normal basement membranes and podocytes, no osmiophilic immune deposits. (bar = 10 μm).

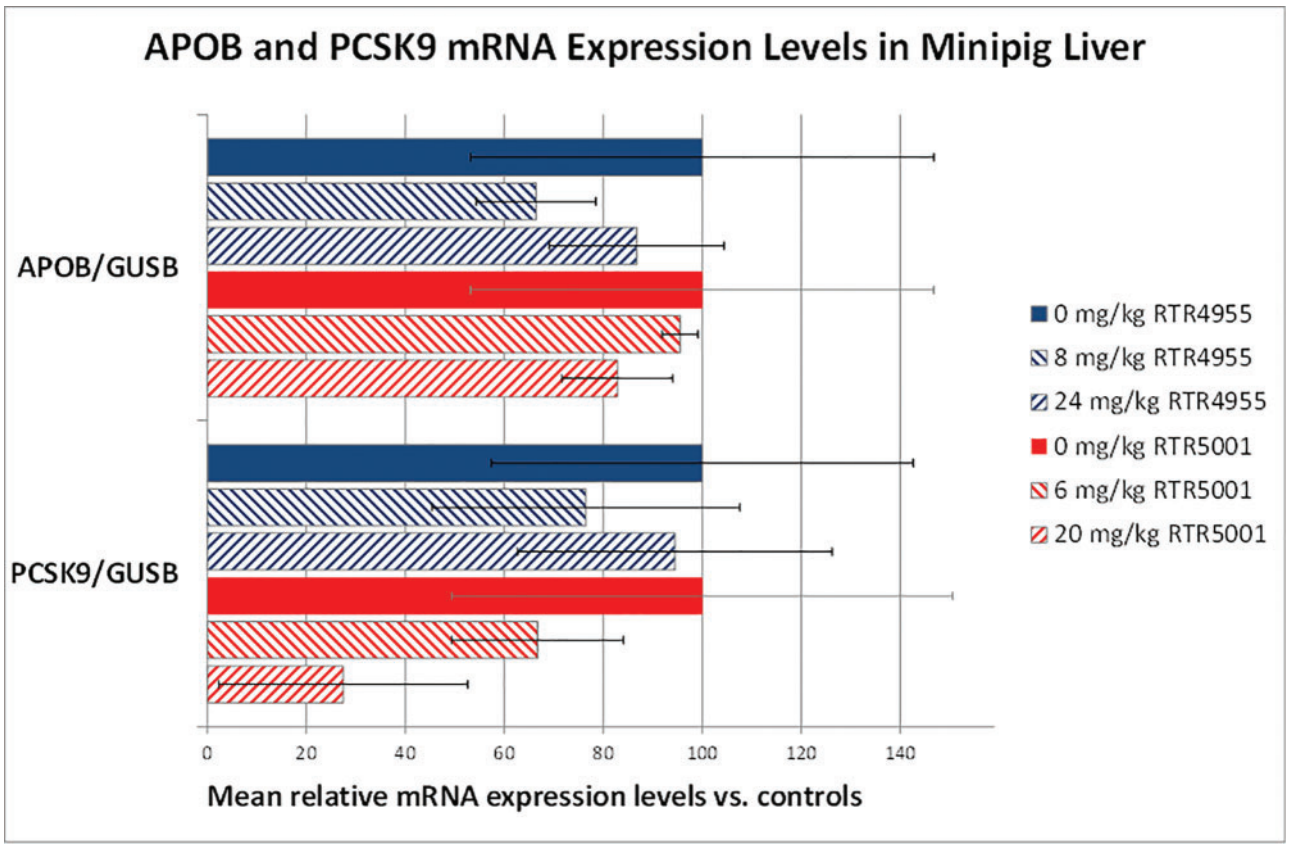

FIG. 8. Mean APOB and PCSK9 mRNA gene expression levels in minipig (N = 3 with ±SD) liver relative to the house-keeping gene beta glucuronidase (GUSB) and relative to mean gene expression of the control group after subcutaneous dosing of RTR4955 or RTR5001. PCSK9 mRNA levels were dose-dependently decreased after administration of RTR5001 but not RTR4955. No changes in APOB mRNA levels were observed after administration of RTR5001 or RTR4955.

dosing with RTR5001, whereas APOB mRNA hepatocellular expression was not altered when compared with controls (Figure 8). Correspondingly, after repeated subcutaneous dosing with RTR5001, LDL cholesterol levels were decreased by up to 53% when compared with controls and pretest levels, thereby confirming a direct pharmacodynamic effect of RTR5001 in minipig livers.

After dosing with RTR4955, neither an effect on APOB mRNA nor PCSK9 mRNA hepatocellular expression (Figure 8) nor cholesterol levels could be identified.

By in-situ hydridization a reduced PCSK9 mRNA expression after RTR5001 dosing was confirmed (Figure 9A and B). No such difference could be identified for APOB mRNA expression levels when compared with control liver tissue samples (Figure 9C and D).

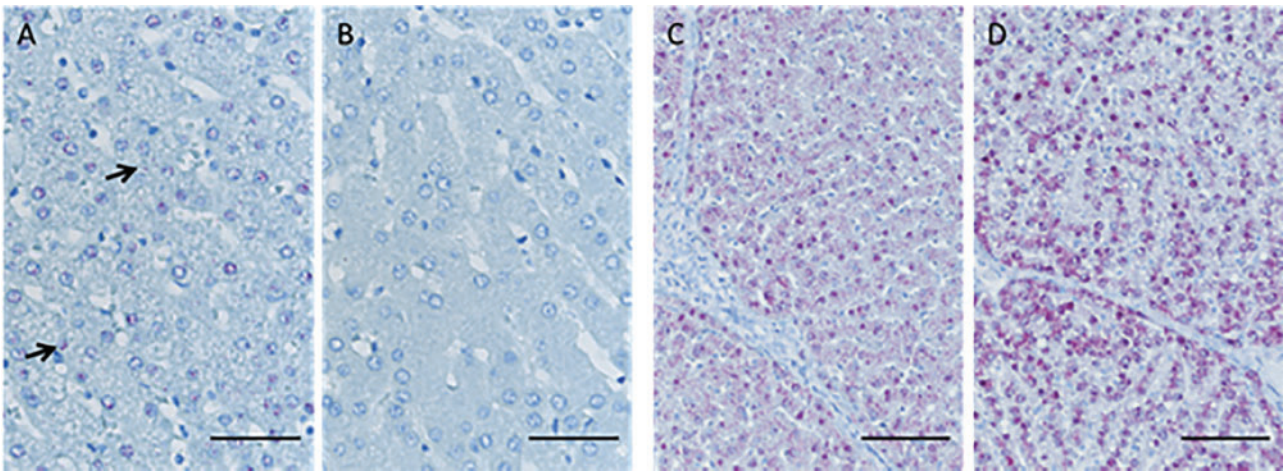

FIG. 9. *In situ* hybridization for detection of PCSK9 or APOB mRNA expression in minipig liver tissue, indicated as red dots with hematoxylin counterstain. A, Minimal PCSK9 expression in control minipig B, No PCSK9 expression in minipig dosed at 20 mg/kg RTR5001 (scale bar = 50 μm) C, Medium to marked APOB expression in control minipig D, Similar amount of APOB expression in minipig dosed at 24 mg/kg RTR4955 compared to control (scale bar = 100 μm).

Minimal to mild cytoplasmic staining for PCSK9 was present in hepatocytes of control minipigs and no or only minimal staining was present in minipigs dosed with 20 mg/kg RTR5001, confirming target engagement in the minipig. Moderate to marked cytoplasmic staining for APOB was present in control minipigs and minipigs dosed with RTR4955, indicating no effect of the LNA SSO on the APOB mRNA expression.

DISCUSSION

Administration of the 4 LNA SSOs resulted in similar clinical findings in minipigs as in NHPs. An overview of the complete response pattern is presented for both non-rodent species, minipig and NHP, for all four different SSO LNAs in Table 1. Trends for clinical pathology changes are considered crucial to correlate with histopathologic findings. After multiple dosing, two high-dose animals for both NHPs and minipigs were sacrificed for humane reasons (**Table 1**). In addition, minipigs showed similar exposure and very good comparability in toxicity profile versus NHPs, with no additional on- or off-target pharmacology or toxicities (**Table 1**). Effects on the coagulation, renal, and complement systems were also similar to those in NHPs.

Overall, the toxicity profile of the LNA SSOs appears to be similar in minipigs and NHPs, and typical of the class-wide toxicity profile of SSOs (Frazier *et al.*, 2014; Koch and Ørum, 2008), with kidney, liver and lymphoid tissues being the main target tissues of toxicity. While some of these effects are hybridization-independent (eg, pro-inflammatory or plasma protein effects) (Henry *et al.*, 2008), the mechanism for others (eg, hepatotoxicity) is still uncertain but may also involve off-target hybridization (Burel *et al.*, 2016).

The pharmaco-/toxicokinetic behavior of the different LNA SSOs was also similar in the minipig and NHPs. As in other species, plasma exposure increased roughly dose-proportionally, and SSOs were rapidly cleared from circulation (Levin *et al.*, 2008). In both species, LNA SSOs are distributed and taken up by peripheral tissues such as the liver and kidney. For the majority of the investigated LNA SSOs there was an exposure saturation in the minipig kidney; generally kidney exposure of the cortex was markedly higher than the liver, as shown previously (Geary *et al.*, 2015; Straarup *et al.*, 2010).

In minipigs dosed intravenously with RTR2996, we observed a transient increase in PT and APTT, and a decrease in total complement. Corresponding clinical signs, including prolonged bleeding and red discoloration of parts of the body, were also transient and reversed within a few minutes after administration. In NHPs, RTR2996 caused coagulation and complement activation; this has been described with other LNA SSOs (Henry *et al.*, 2014; Hildebrandt-Eriksen *et al.*, 2012; Koch and Ørum, 2008) but has not previously been described in minipigs (Henry *et al.*, 2016). In NHPs, activation of the complement system was reported with threshold SSO plasma levels of 70–80 μg/mL (Henry *et al.*, 2014). In our minipig study, activation of the complement system was seen at plasma C_{max} values of approximately 500 μg/mL RTR2996. Although this warrants more data, this finding could suggest a lower sensitivity of minipigs to this liability than NHPs and therefore possibly a higher relevance to human safety assessment since NHPs are known to be overpredictive (Henry *et al.*, 2016). With the confirmed occurrence of acute PT and APTT prolongations after high intravenous doses in both species, this effect is likely also relevant in terms of human safety, even if clinical plasma peak concentrations are often below NHP thresholds (Crooke *et al.*, 2016).

One factor for choosing a relevant species for preclinical safety studies is its ability to capture pharmacological effects (eg, exaggerated pharmacology) of a drug development candidate, which has been a factor in the historical preference for NHPs for biotechnology-derived and oligonucleotide therapeutics. The recent sequencing of the minipig genome was essential for considering the minipig as a potential alternative non-rodent species. As in NHPs, we showed dose-related target engagement, a pharmacodynamic effect and a decrease in LDL cholesterol after repeated dosing with RTR5001 in minipigs (Lindholm *et al.*, 2012). PCSK9 mRNA expression in minipig livers was markedly reduced after RTR5001 administration, confirming pharmacodynamic activity, despite the single mismatch. In contrast, RTR4955 neither altered PCSK9 nor APOB mRNA nor cholesterol levels. These differences are likely due to different positions of the single mismatch to the minipig genome in the LNA SSO sequences. The central mismatch in RTR4955 is expectedly more detrimental on the target regulation than the end-standing mismatch in RTR5001, suggesting that for RTR4955, this region is critical for RNaseH recruitment and cleavage of target mRNA.

After clearance from the circulation, SSOs accumulated in liver Kupffer cells, lymph nodes and, most significantly, in the

TABLE 1. Overview of Main Observations in Minipig and NHP After Dosing With RTR5001, RTR4955, RTR3649 and RTR2996 (Gebert et al., 2014; Hildebrandt-Eriksen et al., 2012; Koch and Ørum, 2008; Lindholm et al., 2012; data on file, F. Hoffmann-La Roche Ltd., 2017)

	RTR5001		RTR4955		RTR3649		RTR2996	
Parameter	Minipig	NHP	Minipig	NHP	Minipig	NHP	Minipig	NHP
Dose levels	0, 6, 20 mg/kg (s.c.)	0, 6, 20 mg/kg (s.c.)	0, 8, 24 mg/kg (s.c.)	0, 8, 24 mg/kg (s.c.)	0, 3, 12 and 48 mg/kg (s.c.)	0, 3, 12 and 48 mg/kg (i.v.)	0, 5, 15, and 45 mg/kg (i.v.)	0, 3, 20, and 60 mg/kg (i.v.)
Dosing days	1, 6, 11 and 16	1, 6, 11 and 16	1, 6, 11 and 16	1, 6, 11 and 16	1, 4, 8, 11, 15, 18, 22, 25, 29	1, 4, 8, 11, 15, 18, 22, 25, 28	1, 3, 5, 7, 9, 11, 13, 15	1, 3, 5, 7, 9, 11, 13, 15
Mortality	–	–	1 humane killed at 24 mg/kg with tubular lesions and glomerulonephritis	1 humane killed at 24 mg/kg with hemorrhages, edema and necrosis of cecum, incl. liver and kidney changes	–	–	1 humane killed at 45 mg/kg with more severe kidney changes	1 humane killed at 60 mg/kg due to liver and kidney changes
Hematology	–	↑ WBC, neutrophils, mononocytes at 20 mg/kg	↑ Neutrophils and monocytes at 24 mg/kg	↑ Reticulo- and monocytes at 24 mg/kg	–	–	↓ Rbc, lymphocytes and reticulocytes at 45 mg/kg	↑ Monocytes at 60 mg/kg
Coagulation	–	–	↑ Fibrinogen at 24 mg/kg	↑ Fibrinogen at ≥8 mg/kg	↑ PT and APTT at ≥ 12 mg/kg	↑ PT and APTT at ≥ 12 mg/kg	↑ PT and APTT at 45 mg/kg associated with flushing of limbs, ear and nose	↑ PT and APTT at ≥ 20 mg/kg
Clinical Chemistry	↓ CHOL, LDL, triglyceride at 20 mg/kg; ↑ Crea in 1 of 3 and BUN at 20 mg/kg	↓ CHOL, triglyceride at 20 mg/kg, LDL at ≥ 6 mg/kg	↑ AST, GDH, Crea and BUN at 24 mg/kg	↑ AST, GGTP, Crea and BUN at ≥ 8 mg/kg, ↓ CHOL, LDL, HDL, triglyceride at ≥ 8 mg/kg	↓ CHOL, HDL, LDL and triglyceride at ≥ 12 mg/kg	↓ CHOL, HDL, LDL at ≥ 3 mg/kg; ↑ ALP at 48 mg/kg; ↑ ALT and AST during recovery	↑ CHOL, CREA, BUN, total protein, albumin, globulin, AST, ALT, GGTP, SDH at 45 mg/kg	↑ ALT, AST, CHOL, BUN, CREA, triglyceride at 60 mg/kg, ↓ albumin and A/G at 60 mg/kg
Urinalysis	↑ Na/Crea & Ca/Crea at 20 mg/kg	–	↑ Volume, NAG, Na/Crea, Ca/Crea, Cl/Crea at 24 mg/kg	Hematuria, proteinuria, leukocytes at ≥ 8 mg/kg	–	–	↑ Volume in 1 of 3 at ≥ 15 mg/kg, protein at 45 mg/kg	↑ Volume at 60 mg/kg and protein at ≥ 20 mg/kg
Organ weight	↑ Kidney at 20 mg/kg	–	↑ Kidney at ≥ 8 mg/kg	↑ Liver and kidney at 24 mg/kg	↑ Liver and kidney at 48 mg/kg	↑ Liver at 48 mg/kg	↑ Liver and kidney at ≥ 5 mg/kg	↑ Kidney and spleen at ≥ 6 mg/kg and liver at ≥ 20 mg/kg
Exposure Kidney cortex	0, 164, 555 μg/g at 0, 6, 20 mg/kg, respectively	0, 386, 602 μg/g at 0, 6, 20 mg/kg, respectively	0, 144, 147 μg/g at 0, 8, 24 mg/kg, respectively	0, 120, 154 μg/g at 0, 8, 24 mg/kg, respectively	0, 643, 1220, 1580 μg/g at 0, 3, 12, 48 mg/kg, respectively	0, 374, 664, 1550 μg/g at 0, 3, 12, 48 mg/kg, respectively	0, 1217, 4237, 5703 μg/g at 0, 5, 15, 45 mg/kg, respectively	Not examined

TABLE 1. (continued)

	RTR5001		RTR4955		RTR3649		RTR2996	
Parameter	Minipig	NHP	Minipig	NHP	Minipig	NHP	Minipig	NHP
Exposure Liver	0, 38, 74 μg/g at 0, 6, 20 mg/kg, respectively	0, 65, 177 μg/g at 0, 6, 20 mg/kg, respectively	0, 32, 82 μg/g at 0, 8, 24 mg/kg, respectively	0, 46, 85 μg/g at 0, 8, 24 mg/kg, respectively	0, 160, 462, 550 μg/g at 0, 3, 12, 48 mg/kg, respectively	0, 68, 293, 551 μg/g at 0, 3, 12, 48 mg/kg, respectively	0, 292, 897, 2283 μg/g at 0, 5, 15, 45 mg/kg, respectively	0, 203, 500, 1042 μg/g at 0, 3, 20, 60 mg/kg, respectively
Histopathology								
Kidney	PAS negative granules, tubular dilatation, degeneration/regeneration in 2 of 3 at 20 mg/kg	Basophilic tubular granules at ≥ 6 mg/kg, tubular dilatation/atrophy in 1 of 3 at 20 mg/kg	Tubular dilatation, degeneration/regeneration at ≥ 8 mg/kg	Tubular single cell necrosis and tubular dilatation and basophilia at ≥ 8 mg/kg	Basophilic granules and tubular degeneration at ≥ 12 mg/kg	Tubular cell vacuolation and in 1 of 6 tubular single cell necrosis at 48 mg/kg	Basophilic granules, tubular degeneration/regeneration at ≥ 15 mg/kg, hyaline casts at 45 mg/kg	Basophilic granules, tubular vacuolation/degeneration/necrosis/hypertrophy, intratubular hemorrhages, perivascular tubular necrosis at ≥ 20 mg/kg
Liver	Single cell necrosis/apoptosis in 1 of 3 at 20 mg/kg	–	Hepatocellular vacuolation, single cell necrosis in 1 of 3 at 24 mg/kg	Hepatocellular vacuolation at ≥ 8 mg/kg, hypertrophy and necrosis associated with mononuclear cell infiltration	Basophilic granules in Kupffer cells at 48 mg/kg, hepatocellular cytoplasmic rarefaction at ≥ 12 mg/kg	Basophilic granules/hypertrophy in Kupffer cells at ≥ 12 mg/kg, hepatocellular cytoplasmic change at ≥ 3 mg/kg; and hepatocellular apoptosis in 1 of 6 at 48 mg/kg	Basophilic granules in Kupffer cells and hepatocellular hypertrophy at ≥ 15 mg/kg, single cell necrosis/apoptosis, Kupffer cell hyperplasia at 45 mg/kg	Basophilic granules in Kupffer cells at ≥ 6 mg/kg, hepatocyte degeneration in 1 of 6 at 60 mg/kg and hepatocellular necrosis in 1 of 6 at 20 mg/kg
Lymph nodes	Vacuolated macrophages at ≥ 6 mg/kg	Sinus histiocytosis (vacuolated/stippled) at ≥ 6 mg/kg	Vacuolated macrophages at ≥ 8 mg/kg	Sinus histiocytosis (vacuolated/stippled) at ≥ 8 mg/kg	Not examined	Vacuolated macrophages at ≥ 3 mg/kg	Vacuolated macrophages at ≥ 5 mg/kg	Foamy macrophages, ↑ cellularity of paracortex at ≥ 6 mg/kg
s.c. injection sites	↑ Severity of inflammation, necrosis and/or edema, hemorrhages	↑ Severity of inflammation, edema and hemorrhages	↑ Hemorrhages; inflammation (similar to controls)	↑ Hemorrhages and acute inflammation	Perivascular infiltration (all doses), inflammatory cell infiltrate, ↑ hemorrhage and fibroplasia at 48 mg/kg	Not applicable (i.v. dosing)	Not applicable (i.v. dosing)	Not applicable (i.v. dosing)

TABLE 1. (continued)

Parameter	RTR5001		RTR4955		RTR3649		RTR2996	
	Minipig	NHP	Minipig	NHP	Minipig	NHP	Minipig	NHP
Additional organs				Monunuclear cell infiltrate and necrosis in heart of 1 of 3 at 24 mg/kg; hemorrhages in cecum, colon and lung at ≥ 8 mg/kg	Not examined			↓ Cellularity of adrenal glands at ≥ 20 mg/kg, ↑ cellularity of PALS at ≥ 6 mg/kg and marginal zone of spleen at 60 mg/kg, ↑ lymphocytic infiltration of the salivary gland at ≥ 6 mg/kg, ↓ cellularity of thymic cortex at 60 mg/kg

Abbreviations: A/G, albumin/globulin ratio; ALP, alkaline phosphatase; APTT, activated partial thromboplastin time; AST, aspartate aminotransferase; BUN, blood urea nitrogen; Ca, calcium; CHOL, total cholesterol; Cl, chloride; Crea, creatinine; GDH, glutamate dehydrogenase; GGTP, gamma-glutamyl transpeptidase; Hb, hemoglobin; Hct, hematocrit; HDL, high density lipoprotein; i.v., intravenous; LDL, low density lipoprotein; Na, sodium; NAG, N-acetyl-beta-D-glucosaminidase; PAS, Periodic acid–Schiff–diastase staining; PALS, periarteriolar lymphoid sheaths; PT, partial prothombin time; Rbc, red blood cells; s.c., subcutaneous; SDH, sorbitol dehydrogenase; WBC, white blood cells.

kidney. Accumulation of LNA SSOs in the proximal tubular cells of the minipig kidney resulted in the presence of cytoplasmic basophilic granules, similar to that previously shown in rodents and NHPs (Frazier *et al.*, 2014; Hildebrandt-Eriksen *et al.*, 2012; Koch and Ørum, 2008). Additionally, in the minipig, we observed degenerative changes of the renal tubular cells previously identified in NHP studies (Henry *et al.*, 2012; Koch and Ørum, 2008; Monteith *et al.*, 1999). In the minipig, RTR3649 produced minimal to mild tubular degeneration in the kidney, whereas in NHPs, vacuolation of tubular cells was reported (Hildebrandt-Eriksen *et al.*, 2012). In minipigs, RTR5001 produced degenerative/regenerative changes in the kidney; no adverse biochemical or histopathologic findings were observed in NHPs (Lindholm *et al.*, 2012; van Poelgeest *et al.*, 2013). In a human trial with RTR5001, one case of acute kidney injury was reported in a healthy volunteer who received three once-weekly doses of 5 mg/kg, with multifocal tubular necrosis/degeneration and evidence of drug accumulation (van Poelgeest *et al.*, 2013) on biopsy. These findings were similar to those in minipigs given RTR5001. Degenerative/regenerative changes of the renal tubular cells were similar in minipigs and NHPs dosed with RTR4955 and RTR2996, although severity was greater with RTR4955 in the minipig. In addition, one minipig dosed with RTR4955 showed a mesangioproliferative glomerulonephritis, a lesion not previously observed in NHPs for the four LNA SSOs. Although no electron-dense deposits along the basal membranes were observed with TEM investigations, the lesion showed similar characteristics to those described previously (Frazier *et al.*, 2014). Therefore, the pathogenesis—not fully clarified—may be related to a dysfunction of the alternative complement pathway. Regardless of the mechanism, minipigs may be more sensitive to kidney toxicity at high doses than NHPs.

As commonly observed in NHPs and rodents, basophilic cytoplasmic granules were observed in the Kupffer cells in minipigs dosed with RTR3649 and RTR2996. Immunohistochemistry and *in-situ* hybridization showed this was due to SSO accumulation. Hepatocellular single cell necrosis/apoptosis, correlating with increased serum transaminase activities, were observed in minipigs administered RTR2996, in one minipig administered RTR5001, and another one administered RTR4955. Similar changes were seen in NHPs administered RTR4955 and RTR2996 (Koch and Ørum, 2008; Straarup *et al.*, 2010). In clinical studies, RTR4955 caused a mild increase in serum transaminase activities in some subjects, and a dose-limiting increase in serum transaminase activities occurred in two patients treated with RTR2996 4 mg/kg 3 times per week for two weeks (Tilly *et al.*, 2007).

Vacuolated macrophages were observed in minipig lymph nodes, including the draining lymph node of the injection site, similar to those described in other species (Frazier *et al.*, 2014). Immunohistochemistry and *in-situ* hybridization showed the presence of the LNA SSO in these vacuolated macrophages. These so-called foamy/stippled macrophages were described previously in NHPs (Hildebrandt-Eriksen *et al.*, 2012).

During clinical trials, and after subcutaneous dosing of SSOs, ISRs such as erythema, ulceration, necrosis and hyperpigmentation have been observed (van Meer *et al.*, 2016; van Poelgeest *et al.*, 2015). Although minipig skin shows similarities to human anatomy, physiology, and biochemistry (Forster *et al.*, 2010; Mahl *et al.*, 2006) and has been considered a model to predict human cutaneous reactions, no acute or gross clinical observations were made in either the minipig or NHPs. Histopathologically, subcutaneous dosing of RTR5001 in minipigs resulted in an increased inflammation in the subcutis, characterized by the presence of macrophages, lymphocytes,

granulocytes, edema, hemorrhages, and necrosis. A tendency to recovery from these ISRs was shown by comparing the previous and last injection sites. Inflammatory changes were identified at the injection sites of control animals and minipigs administered RTR4955. Increased severity and incidence of hemorrhages were noted in RTR4955-dosed minipigs. RTR3649 caused perivascular inflammatory cell infiltration of mainly lymphocytes and eosinophilic granulocytes as well as necrosis at the injection sites in the minipig. However, as NHPs were dosed intravenously in the duration-matching study, a direct comparison cannot be made. Subcutaneous injection of RTR5001 and RTR4955 to NHPs caused inflammation, with predominant infiltration of neutrophils and formation of edema in the subcutis. In humans, SSOs are associated with ISRs of varying severity when administered subcutaneously (van Meer *et al.*, 2016); lesion severity is dose-dependent, and some SSOs cause persistent lesions (van Meer *et al.*, 2016; van Poelgeest et al., 2015). Consequently, although no overt ISRs were evident during the in-life phase in our preclinical studies, the histopathological examination of injection sites should still be considered, as data suggest similarities to reactions described in humans (van Meer *et al.*, 2016).

In conclusion, our data from four LNA SSOs support the use of the minipig in the preclinical safety assessment of this class of molecules. We demonstrated that the minipig shows a similar safety profile as the NHP for four different molecules upon subacute exposure. No additional off-target pharmacological effects or non-hybridization-dependent toxicities were identified. Consequently, the number of NHPs that are currently used in preclinical safety assessment of SSOs could be reduced. Finally, species selection should always maximize the likelihood of identifying responses that are similar to those expected in humans. Therefore, the design of respective cross-reactive SSOs to the minipig genome, as well as the pharmacologic activity and a similarity in the target distribution to humans is essential to ultimately select the minipig as the non-rodent species in preclinical safety investigation.

SUPPLEMENTARY DATA

Supplementary data are available at *Toxicological Sciences* online.

ACKNOWLEDGMENTS

This research project would not have been possible without the highly skilled technical support of F. Hoffmann-La Roche personnel from in vivo, clinical pathology, histopathology, bioanalytical, toxicokinetics laboratories as well as comparative medicine which is gratefully acknowledged. Editorial assistance was provided by Meridian HealthComms, funded by F. Hoffmann-La Roche Ltd. Special thanks to Michael Winter for his expert support in clinical pathology. All authors, except MJM acknowledge that they are employed by F. Hoffmann-La Roche, Ltd.

FUNDING

This work was supported and funded by F. Hoffmann-La Roche Ltd, Basel, Switzerland. All authors, except MJM, are employed by F. Hoffmann-La Roche Ltd.

REFERENCES

Atzpodien, E. A., Jacobsen, B., Funk, J., Altmann, B., Silva Munoz, M. A., Singer, T., Gyger C., Hasler, P., and Maloca, P. (2016). Advanced Clinical Imaging and Tissue-based Biomarkers of the Eye for Toxicology Studies in Minipigs. *Toxicol Pathol*. **44**, 398–413.

Bode, G., Clausing, P., Gervais, F., Loegsted, J., Luft, J., Nogues, V., Sims, J., and Steering Group of the, R. P. (2010). The utility of the minipig as an animal model in regulatory toxicology. *J. Pharmacol. Toxicol. Methods* **62**, 196–220.

Burdick, A. D., Sciabola, S., Mantena, S. R., Hollingshead, B. D., Stanton, R., Warneke, J. A., Zeng, M., Martsen, E., Medvedev, A., Makarov, S. S., *et al.* (2014). Sequence motifs associated with hepatotoxicity of locked nucleic acid–modified antisense oligonucleotides. *Nucleic Acids Res*. **42**, 4882–4891.

Burel, S. A., Hart, C. E., Cauntay, P., Hsiao, J., Machemer, T., Katz, M., Watt, A., Bui, H. H., Younis, H., Sabripour, M., *et al.* (2016). Hepatotoxicity of high affinity gapmer antisense oligonucleotides is mediated by RNase H1 dependent promiscuous reduction of very long pre-mRNA transcripts. *Nucleic Acids Res*. **44**, 2093–2109.

Cai, H., Santiago, F. S., Prado-Lourenco, L., Wang, B., Patrikakis, M., Davenport, M. P., Maghzal, G. J., Stocker, R., Parish, C. R., Chong, B. H., *et al.* (2012). DNAzyme targeting c-jun suppresses skin cancer growth. *Sci. Transl. Med*. **4**, 139ra82.

Crooke, S. T., Baker, B. F., Kwoh, T. J., Cheng, W., Schulz, D. J., Xia, S., Salgado, N., Bui, H. H., Hart, C. E., Burel, S. A., *et al.* (2016). Integrated safety assessment of 2'-O-methoxyethyl chimeric antisense oligonucleotides in nonhuman primates and healthy human volunteers. *Mol. Ther*. **10**, 1771–1782.

Danis, R., Criswell, M., Orge, F., Wancewicz, E., Stecker, K., Henry, S., and Monia, B. (2003). Intravitreous anti-raf-1 kinase antisense oligonucleotide as an angioinhibitory agent in porcine preretinal neovascularization. *Curr. Eye Res*. **26**, 45–54.

Durig, J., Duhrsen, U., Klein-Hitpass, L., Worm, J., Hansen, J. B., Orum, H., and Wissenbach, M. (2011). The novel antisense Bcl-2 inhibitor SPC2996 causes rapid leukemic cell clearance and immune activation in chronic lymphocytic leukemia. *Leukemia* **25**, 638–647.

Engelhardt, J. A., Fant, P., Guionaud, S., Henry, S. P., Leach, M. W., Louden, C., Scicchitano, M. S., Weaver, J. L., Zabka, T. S., and Frazier, K. S. (2015). Scientific and Regulatory Policy Committee Points-to-consider Paper*: Drug-induced Vascular Injury Associated with Nonsmall Molecule Therapeutics in Preclinical Development: Part 2. Antisense Oligonucleotides. *Toxicol. Pathol*. **43**, 935–944.

FDA Briefing Document (2012). FDA Briefing Document, NDA 203568, Mipomersen. Available at: http://www.fda.gov/downloads/AdvisoryCommittees/CommitteesMeetingMaterials/Drugs/EndocrinologicandMetabolicDrugsAdvisoryCommittee/UCM323927.pdf. Accessed October 26, 2016.

Forster, R., Bode, G., Ellegaard, L., and van der Laan, J. W. (2010). The RETHINK project on minipigs in the toxicity testing of new medicines and chemicals: Conclusions and recommendations. *J. Pharmacol. Toxicol Methods* **62**, 236–242.

Frazier, K. S. (2015). Antisense oligonucleotide therapies: The promise and the challenges from *A Toxicologic Pathologist's Perspective*. *Toxicol. Pathol*. **43**, 78–89.

Frazier, K. S., Sobry, C., Derr, V., Adams, M. J., Besten, C. D., Kimpe, S. D., Francis, I., Gales, T. L., Haworth, R., Maguire, S. R., *et al.* (2014). Species-specific inflammatory responses as a primary component for the development of glomerular lesions in mice and monkeys following chronic administration

of a second-generation antisense oligonucleotide. *Toxicol. Pathol.* **42**, 923–935.

Frieden, M., and Orum, H. (2008). Locked nucleic acid holds promise in the treatment of cancer. *Curr. Pharm. Des.* **14**, 1138–1142.

Ganderup, N. C., Harvey, W., Mortensen, J. T., and Harrouk, W. (2012). The minipig as nonrodent species in toxicology—where are we now? *Int. J. Toxicol.* **31**, 507–528.

Geary, R. S., Norris, D., Yu, R., and Bennett, C. F. (2015). Pharmacokinetics, biodistribution and cell uptake of antisense oligonucleotides. *Adv. Drug Deliv. Rev.* **87**, 46–51.

Gebert, L. F., Rebhan, M. A., Crivelli, S. E., Denzler, R., Stoffel, M., and Hall, J. (2014). Miravirsen (SPC3649) can inhibit the biogenesis of miR-122. *Nucleic Acids Res.* **42**, 609–621.

Heckel, T., Schmucki, R., Berrera, M., Ringshandl, S., Badi, L., Steiner, G., Ravon, M., Kung, E., Kuhn, B., Kratochwil, N. A., *et al.* (2015). Functional analysis and transcriptional output of the Gottingen minipig genome. *BMC Genomics* **16**, 932.

Henry, S. P., Jagels, M. A., Hugli, T. E., Manalili, S., Geary, R. S., Giclas, P. C., and Levin, A. A. (2014). Mechanism of alternative complement pathway dysregulation by a phosphorothioate oligonucleotide in monkey and human serum. *Nucleic Acid Ther.* **24**, 326–335.

Henry, S. P., Johnson, M., Zanardi, T. A., Fey, R., Auyeung, D., Lappin, P. B., and Levin, A. A. (2012). Renal uptake and tolerability of a 2′-O-methoxyethyl modified antisense oligonucleotide (ISIS 113715) in monkey. *Toxicology* **301**, 13–20.

Henry, S. P., Kim, T. W., Kramer-Stickland, K., Zanardi, T. A., Fey, R. A., and Levin, A. A. (2008). Toxicologic proprieties of 2′-O-methoxyethyl chimeric antisense inhibitors in animals and man. In *Antisense Drug Technology: Principles, Strategies, and Applications*, 2nd ed. (S. T. Crooke, Ed.), pp. 327–363. CRC Press, Boca Raton.

Henry, S. P., Monteith, D., Bennett, F., and Levin, A. A. (1997). Toxicological and pharmacokinetic properties of chemically modified antisense oligonucleotide inhibitors of PKC-alpha and C-raf kinase. *Anticancer Drug Des.* **12**, 409–420.

Henry, S. P., Seguin, R., Cavagnaro, J., Berman, C., Tepper, J., and Kornbrust, D. (2016). Considerations for the characterization and interpretation of results related to alternative complement activation in monkeys associated with oligonucleotide-based therapeutics. *Nucleic Acid Ther.* **4**, 210–215.

Hildebrandt-Eriksen, E. S., Aarup, V., Persson, R., Hansen, H. F., Munk, M. E., and Orum, H. (2012). A locked nucleic acid oligonucleotide targeting microRNA 122 is well-tolerated in cynomolgus monkeys. *Nucleic Acid Ther.* **22**, 152–161.

Iyer, R. P., Marquis, J., and Bonnez, W. (2002). ORI-1001 Anti-papilloma virus oligonucleotide. *Drugs Future* **27**, 546–557.

Koch, T., and Ørum, H. (2008). Locked nucleic acid. In *Antisense Drug Technology: Principles, Strategies, and Applications*, 2nd ed. (S. T. Crooke, Ed.), pp. 519–564. CRC Press, Boca Raton.

Lee, R. G., Fu, W., Graham, M. J., Mullick, A. E., Sipe, D., Gattis, D., Bell, T. A., Booten, S., and Crooke, R. M. (2013). Comparison of the pharmacological profiles of murine antisense oligonucleotides targeting apolipoprotein B and microsomal triglyceride transfer protein. *J. Lipid Res.* **54**, 602–614.

Levin, A. A., Yu, R. Z., and Geary, R. S. (2008). Basic principles of the pharmacokinetics of antisense oligonucleotide drugs. In *Antisense Drug Technology: Principles, Strategies, and Applications*, 2nd ed. (S. T. Crooke, Ed.), pp. 183–215. CRC Press, Boca Raton.

Lindholm, M. W., Elmen, J., Fisker, N., Hansen, H. F., Persson, R., Moller, M. R., Rosenbohm, C., Orum, H., Straarup, E. M., and Koch, T. (2012). PCSK9 LNA antisense oligonucleotides induce sustained reduction of LDL cholesterol in nonhuman primates. *Mol. Ther.* **20**, 376–381.

Mahl, J. A., Vogel, B. E., Court, M., Kolopp, M., Roman, D., and Nogues, V. (2006). The minipig in dermatotoxicology: methods and challenges. *Exp. Toxicol. Pathol.* **57**, 341–345.

Mehta, R. C., Stecker, K. K., Cooper, S. R., Templin, M. V., Tsai, Y. J., Condon, T. P., Bennett, C. F., and Hardee, G. E. (2000). Intercellular adhesion molecule-1 suppression in skin by topical delivery of anti-sense oligonucleotides. *J. Invest. Dermatol.* **115**, 805–812.

Monteith, D. K., Horner, M. J., Gillett, N. A., Butler, M., Geary, R., Burckin, T., Ushiro-Watanabe, T., and Levin, A. A. (1999). Evaluation of the renal effects of an antisense phosphorothioate oligodeoxynucleotide in monkeys. *Toxicol. Pathol.* **27**, 307–317.

Morton, D. M. (1998). Importance of species selection in drug toxicity testing. *Toxicol. Lett.* **102–103**, 545–550.

Perry, C. M., and Balfour, J. A. (1999). Fomivirsen. *Drugs* **57**, 375–380.

Russell, W. M. S., and Burch, R. L. (1959). The principles of humane experimental technique. London (UK): Metheuen.

Stein, C. A., Hansen, J. B., Lai, J., Wu, S., Voskresenskiy, A., Hog, A., Worm, J., Hedtjarn, M., Souleimanian, N., Miller, P., *et al.* (2010). Efficient gene silencing by delivery of locked nucleic acid antisense oligonucleotides, unassisted by transfection reagents. *Nucleic Acids Res.* **38**, e3.

Straarup, E. M., Fisker, N., Hedtjarn, M., Lindholm, M. W., Rosenbohm, C., Aarup, V., Hansen, H. F., Orum, H., Hansen, J. B., and Koch, T. (2010). Short locked nucleic acid antisense oligonucleotides potently reduce apolipoprotein B mRNA and serum cholesterol in mice and non-human primates. *Nucleic Acids Res.* **38**, 7100–7111.

Tilly, H., Coiffier, B., Michallet, A. S., Radford, J. A., Geisler, C. H., Gadeberg, O., Dalseg, A., Steenken, E. J., and Worsaae Dalby, L. (2007). Phase I/II study of SPC2996, an RNA antagonist of Bcl-2, in patients with advanced chronic lymphocytic leukemia (CLL). *J. Clin. Oncol.* **25**(18_suppl), 7036–7036.

Vamathevan, J. J., Hall, M. D., Hasan, S., Woollard, P. M., Xu, M., Yang, Y., Li, X., Wang, X., Kenny, S., Brown, J. R., *et al.* (2013). Minipig and beagle animal model genomes aid species selection in pharmaceutical discovery and development. *Toxicol Appl Pharmacol* **270**, 149–157.

van Meer, L., Moerland, M., Gallagher, J., van Doorn, M. B., Prens, E. P., Cohen, A. F., Rissmann, R., and Burggraaf, J. *et al.* (2016) Injection site reactions after subcutaneous oligonucleotide therapy. *Br. J. Clin. Pharmacol.* **82**, 340–51.

van Poelgeest, E. P., Hodges, M. R., Moerland, M., Tessier, Y., Levin, A. A., Persson, R., Lindholm, M. W., Dumong Erichsen, K., Orum, H., Cohen, A. F., *et al.* (2015). Antisense-mediated reduction of proprotein convertase subtilisin/kexin type 9 (PCSK9): A first-in-human randomized, placebo-controlled trial. *Br. J. Clin. Pharmacol.* **80**, 1350–1361.

van Poelgeest, E. P., Swart, R. M., Betjes, M. G., Moerland, M., Weening, J. J., Tessier, Y., Hodges, M. R., Levin, A. A., and Burggraaf, J. (2013). Acute kidney injury during therapy with an antisense oligonucleotide directed against PCSK9. *Am. J. Kidney Dis.* **62**, 796–800.

Veedu, R. N., Burri, H. V., Kumar, P., Sharma, P. K., Hrdlicka, P. J., Vester, B., and Wengel, J. (2010). Polymerase-directed synthesis of C5-ethynyl locked nucleic acids. *Bioorg. Med. Chem. Lett.* **20**, 6565–6568.

Vester, B., and Wengel, J. (2004). LNA (locked nucleic acid): High-affinity targeting of complementary RNA and DNA. *Biochemistry* **43**, 13233–13241.

Wang, F., Flanagan, J., Su, N., Wang, L. C., Bui, S., Nielson, A., Wu, X., Vo, H. T., Ma, X. J., and Luo, Y. (2012). RNAscope: A novel in situ RNA analysis platform for formalin-fixed, paraffin-embedded tissues. *J. Mol. Diagn.* **14**, 22–29.